

# On the Lack of Thermal Emission from the Quiescent Black Hole XTE J1118+480: Evidence for the Event Horizon

Jeffrey E. McClintock, Ramesh Narayan, and George B. Rybicki

*Harvard-Smithsonian Center for Astrophysics, Cambridge, MA 02138, USA*

`jem@cfa.harvard.edu, rnarayan@cfa.harvard.edu, grybicki@cfa.harvard.edu`

## ABSTRACT

A soft component of thermal emission is very commonly observed from the surfaces of quiescent, accreting neutron stars. We searched with *Chandra* for such a surface component of emission from the dynamical black-hole candidate XTE J1118+480 (= J1118), which has a primary mass  $M_1 \approx 8 M_\odot$ . None was found, as one would expect if the compact X-ray source is a bona fide black hole that possesses an event horizon. The spectrum of J1118 is well-fitted by a simple power-law model that implies an unabsorbed luminosity of  $L_x \approx 3.5 \times 10^{30}$  erg s<sup>-1</sup> (0.3–7 keV). In our search for a thermal component, we fitted our *Chandra* data to a power-law model (with slope and  $N_H$  fixed) plus a series of nine hydrogen-atmosphere models with radii ranging from 9/8 to 2.8 Schwarzschild radii. For the more compact models, we included the important effect of self-irradiation of the atmosphere. Because of the remarkably low column density to J1118,  $N_H \approx 1.2 \times 10^{20}$  cm<sup>-2</sup>, we obtained very strong limits on a hypothetical thermal source:  $kT_\infty < 0.011$  keV and  $L_{\infty, \text{th}} < 9.4 \times 10^{30}$  erg s<sup>-1</sup> (99% confidence level). In analogy with neutron stars, there are two possible sources of thermal radiation from a hypothetical surface of J1118: deep crustal heating and accretion. The former mechanism predicts a thermal luminosity that exceeds the above luminosity limit by a factor of  $\gtrsim 25$ , which implies that either one must resort to contrived models or, as we favor, J1118 is a true black hole with an event horizon. In addition to neutron stars, we also consider emission from several exotic models of compact stars that have been proposed as alternatives to black holes. As we have shown previously, accreting black holes in quiescent X-ray binaries are very much fainter than neutron stars. One potential explanation for this difference is the larger and hence cooler surface of an  $8 M_\odot$  compact object that might be masked by the ISM. However, our upper limit on the *total* luminosity of J1118 of  $1.3 \times 10^{31}$  erg s<sup>-1</sup> is far below the luminosities observed for neutron stars. This result strengthens our long-held position that black holes are faint relative to neutron stars because they possess an event horizon.

*Subject headings:* X-ray: stars — binaries: close — accretion, accretion disks — black hole physics — stars: individual (XTE J1118+480)

## 1. Introduction

In principle it is possible to detect the radiation emitted from the surface of any ordinary astronomical body such as a planet or a star of any kind. On the other hand, it is quite impossible to detect any radiation from an event horizon, which is the immaterial surface of infinite redshift that defines a black hole. This is unfortunate because demonstrating the reality of the event horizon is a problem central to physics and astrophysics. Nevertheless, despite the complete absence of any emitted radiation, it is possible to marshal strong circumstantial evidence for the reality of the event horizon. One fruitful approach is based on comparing low mass X-ray binaries (LMXBs) that contain black hole primaries with very similar LMXBs that contain neutron star primaries. In the quiescent state of these systems (McClintock & Remillard 2004), the lack of a stellar surface leads to predictable consequences, such as the faintness of black holes relative to neutron stars (Narayan, Garcia, & McClintock 1997b; Garcia et al. 2001; Narayan, Garcia & McClintock 2002), and also the lack of a thermal component of emission from black holes, which is commonly present in neutron stars (this work). Similarly, in the outburst state, the presence of a surface in the neutron star (NS) systems gives rise to some distinctive phenomena that are absent in the black hole (BH) systems: (1) type I thermonuclear bursts (Narayan & Heyl 2002); (2) high-frequency ( $\sim 1$  kHz) timing noise (Sunyaev & Revnivtsev 2000); and (3) a distinctive spectral component from a boundary layer at the stellar surface (Done & Gierlinski 2003).

In quiescence, almost all accreting neutron stars (e.g., Cen X-4, Aql X-1, and KS 1731-260) display a soft (kT  $\sim 0.1$  keV) thermal component of emission (see §4.2). The source of the thermal energy is uncertain; for example, it may be energy liberated by the impact of accreting matter (Narayan et al. 1997b, 2002) or crustal energy from the star's interior (Brown, Bildsten, & Rutledge 1998; Rutledge et al. 2002b). In any case, however, the observed X-ray luminosities, temperatures and distances of these NSs indicate that one is observing thermal emission from a source of radius  $\sim 10$  km, which is plainly the stellar surface.

On the other hand, no quiescent thermal component of emission has been reported for any of the 15 BH LMXBs (McClintock & Remillard 2004), which is the expected result if they possess an event horizon. These BH spectra are well-represented by a simple power law with photon index  $1.5 < \Gamma < 2.1$  (McClintock & Remillard 2004). However, a soft component of emission might have escaped detection for several reasons. For example, the quiescent BH

LMXBs are fainter, making a soft component more difficult to observe. Also, compared to the surface of a NS, a hypothetical material surface surrounding a  $\sim 10 M_{\odot}$  compact object would be larger and therefore have a correspondingly lower surface temperature.

Herein we search for a thermal component of emission in the quiescent spectrum of XTE J1118+480 (hereafter J1118), a BH LMXB with an extraordinarily high Galactic latitude ( $b = 62^{\circ}$ ) and correspondingly low interstellar absorption:  $N_{\text{H}} \approx 1.2 \times 10^{20} \text{ cm}^{-2}$  (see §2). For this nominal column depth, the transmission of the interstellar medium (ISM) is 70% for the softest X-rays (0.3 keV) that we consider. Thus, J1118 provides a unique opportunity to search for a soft thermal component of X-ray emission. For the purposes of this study, we adopt a mass for the BH primary of  $M_1 = 8 M_{\odot}$  (McClintock et al. 2001a; Wagner et al. 2001; Orosz et al. 2004). The quiescent X-ray luminosity is  $\approx 3.5 \times 10^{30} \text{ erg s}^{-1}$  (0.3–7 keV;  $D = 1.8 \text{ kpc}$ ), which is  $10^{-8.5}$  of the Eddington luminosity (McClintock et al. 2003). Both the luminosity and the photon spectral index,  $\Gamma = 2.02 \pm 0.16$ , are typical for a quiescent BH LMXB with a short orbital period,  $P_{\text{orb}} = 4.1 \text{ hr}$  (McClintock et al. 2003). All of the BH and NS LMXBs that we consider herein are X-ray novae (a.k.a. soft X-ray transients) that undergo bright outbursts lasting several months, which are followed by years or decades of quiescence. During its outburst maximum, J1118 was exceptionally underluminous in the 2–12 keV band,  $L_{\text{x}} \approx 3 \times 10^{35} \text{ erg s}^{-1}$ , compared to the other BH LMXBs in outburst,  $L_{\text{x}} \sim 10^{38} \text{ erg s}^{-1}$  (McClintock & Remillard 2004).

In this work, we determine a strong upper limit on any soft thermal component in the *Chandra* X-ray spectrum of J1118. Using our upper limit on this emission component, and assuming that J1118 possesses a hypothetical material surface, we set stringent temperature and luminosity upper limits on thermal emission from this surface for a wide range of assumed surface radii; we compare these limits to the observed temperatures and luminosities of quiescent NS LMXBs. We conclude that the absence of a soft thermal component of emission in the spectrum of J1118 rules strongly against the presence of a material surface and hence argues for the existence of an event horizon.

This work is organized as follows. In §2 we examine the central question of the column density to J1118, and in §3 we discuss the observations, data analysis and model-fitting techniques. The development and computation of stellar atmospheric models appropriate to a compact and massive star are presented in Appendix A; the models include the effects of self-irradiation for stars so compact as to lie within their own photon spheres. In §4, upper limits on the temperature and luminosity of a thermal component from J1118 are summarized and discussed, and these results are compared to the thermal spectra observed for neutron stars. In §5, we interpret the absence of thermal emission from J1118 in terms of two conventional sources of thermal emission from NSs; in addition we consider emission

from exotic models of massive, compact stars that have been proposed as alternatives to BHs. Our conclusions are summarized in §6. J1118 and the other BHs referred to throughout this work are among the 18 dynamically-confirmed BHs; for a review of the properties of these massive, compact X-ray sources, see McClintock & Remillard (2004).

## 2. Interstellar Absorption

Knowledge of the interstellar absorption is crucial to the determination of the limits on the temperatures and luminosities of the compact objects that are modeled in this work. In this regard, the very high Galactic latitude of J1118 ( $b = 62^\circ$ ) and therefore low interstellar absorption has already been noted (§1). The location of J1118 close to the Lockman Hole (Lockman, Jahoda & McCammon 1986) indicates an expected column density of  $N_{\text{H}} = 0.5 - 1.5 \times 10^{20} \text{ cm}^{-2}$  (see Hynes et al. 2000). As another indicator of low  $N_{\text{H}}$ , J1118 is the only X-ray nova that was observable by the *Extreme Ultraviolet Explorer (EUVE)* during its 9-year mission (Hynes et al. 2000), which is especially remarkable given the faintness of the X-ray source during outburst (§1). The good quality of the EUV spectrum (0.10–0.19 keV) obtained for J1118 (Hynes et al. 2000) strongly attests to the low interstellar absorption, especially when one considers that the transmission of the ISM is only  $\approx 10^{-3}$  at 0.10 keV for a nominal column depth of  $N_{\text{H}} = 1.2 \times 10^{20} \text{ cm}^{-2}$  (see below).

Plainly, the EUV fluxes corrected for interstellar absorption are extremely sensitive to the value assumed for  $N_{\text{H}}$  (Hynes et al. 2000). This fact plus a very complete set of simultaneous observations of J1118 in outburst obtained using UKIRT, *EUVE*, *HST*, *Chandra* and *RXTE* have allowed strong constraints to be placed on  $N_{\text{H}}$ . The one reasonable assumption that must be made is that the *HST* data (1.2–10.7 eV), which are very *insensitive* to the choice of  $N_{\text{H}}$ , represent the Rayleigh-Jeans portion of a cool ( $kT \approx 24 \text{ eV}$ ) accretion disk spectrum, whereas the *EUVE* data (100–190 eV) constitute the Wien portion of this disk spectrum (McClintock et al. 2001b). (The X-ray data extending from 0.24–160 keV correspond to a separate power-law component of emission; McClintock et al. 2001b). The preferred range of  $N_{\text{H}}$  for which the *HST* and *EUVE* data harmonize to form an accretion disk spectrum is  $N_{\text{H}} = 1.0 - 1.3 \times 10^{20} \text{ cm}^{-2}$ . This determination of the column density strongly rules against  $N_{\text{H}} < 0.75 \times 10^{20} \text{ cm}^{-2}$  or  $N_{\text{H}} > 1.6 \times 10^{20} \text{ cm}^{-2}$ . These results have been corroborated by a recent reanalysis of these data and an analysis of much additional multiwavelength data by Chaty et al. (2003) who conclude that  $N_{\text{H}} = 0.80 - 1.30 \times 10^{20} \text{ cm}^{-2}$  with a preferred value of  $N_{\text{H}} = 1.1 \times 10^{20} \text{ cm}^{-2}$ .

In assessing the hydrogen column density to J1118, Frontera et al. (2001) consider results based on radio measurements of H I (Dickey & Lockman 1990), the detection of weak

interstellar Ca II lines (Dubus et al. 2001), and fits to their *Beppo-SAX* X-ray spectra. They conclude that the “most likely range” of  $N_{\text{H}}$  is  $(1-1.5) \times 10^{20} \text{ cm}^{-2}$ . A subsequent *Beppo-SAX* observation indicated a value of  $N_{\text{H}}$  near the low end of this range (Frontera et al. 2003). In conclusion, based on the three independent lines of argument sketched above — namely, the radio results (see Hynes et al. 2000; Dickey & Lockman 1990), the multiwavelength spectral results (McClintock et al. 2001b; Chaty et al. 2003), and the *BeppoSax* spectral fits (Frontera et al. 2001, 2003) — *we adopt  $N_{\text{H}} = 1.2 \times 10^{20} \text{ cm}^{-2}$  as the most likely value of the column density, and  $N_{\text{H}} < 1.6 \times 10^{20} \text{ cm}^{-2}$  as a conservative upper limit.* As we show below, our results are scarcely affected by uncertainties in the column density because the transmission of the ISM is very high even at the lowest energies considered here (e.g., 70% at 0.3 keV for  $N_{\text{H}} = 1.2 \times 10^{20} \text{ cm}^{-2}$ ).

### 3. Observations, Data Analysis, and Model Fitting

The X-ray data were obtained with the Advanced CCD Imaging Spectrometer (ACIS; Garmire et al. 1992) onboard *The Chandra X-ray Observatory* on 2002 January 11 and 12 UT. The data are identical to those described in McClintock et al. (2003; hereafter MNG03). MNG03 used only a 45.8 ks subset of the *Chandra* data that was obtained on January 12 during simultaneous observations made with the *HST* and the MMT. In this work we include an additional 7.7 ks of data that were obtained one day earlier (see MNG03 for details); the analysis of these data was identical to the analysis described previously for the larger data set, and we refer the reader to the discussion in MNG03 for a number of the details, which we omit here. The resulting pair of pulse height spectra and their response files were combined using FTOOLS (Arnaud & Dorman 2003) which yielded a single spectrum and response file with a net exposure time of 53.5 ks and a total of 89 source counts. The predicted number of background counts in the source extraction circle was small, 1.0 counts, and we neglected the background in our spectral analysis. As before, the response file is corrected for the ongoing degradation in the ACIS-S low energy quantum efficiency (MNG03).

The source counts were binned into 12 bins, each with 7–8 counts per bin. As in MNG03, we fitted the pulse height spectrum to several single-component spectral models (Arnaud & Dorman 2003) with interstellar absorption (Balucinska-Church & McCammon 1992), fixing the column density to the value determined in outburst:  $N_{\text{H}} = 1.2 \times 10^{20} \text{ cm}^{-2}$  (see §2). For a power-law model we find a photon index  $\Gamma = 1.92 \pm 0.16$  ( $\chi^2_{\nu} = 1.01$  for 10 dof). This fit is based on  $\chi^2$  statistics with a conventional  $\sqrt{N}$  weighting function, and the results are entirely consistent with those presented in MNG03. As in MNG03, we use this power-law model to represent the observed spectrum throughout this work. However, we note that we

also could have used a bremsstrahlung model with  $kT = 1.63$  keV ( $\chi^2_\nu = 0.98$  for 10 dof). However, some other common thermal models give poor or unacceptable fits to the data. For example, the blackbody model and the Raymond-Smith model (with cosmic abundances) give values of reduced  $\chi^2$  of 1.7 and 2.8 (10 dof), respectively. However, even these models can be fitted satisfactorily if one allows  $N_{\text{H}}$  to vary freely.

In this work, we adopt the following conservative approach. Because we have only 7–8 counts per bin, we use the Gehrels’ weighting function ( $1 + \sqrt{N + 0.75}$ ) in conjunction with  $\chi^2$  statistics, which provides a good approximation to Poisson statistics (Gehrels 1986; Arnaud & Dorman 2003). Using this approach, we refitted the binned data with the power-law model and found the same value for the photon index, although the error was increased somewhat (38%), as expected:  $\Gamma(\text{Gehrels}) = 1.92 \pm 0.23$  ( $\chi^2_\nu = 0.50$  for 10 dof). *The Gehrels’ weighting function gives larger errors and therefore more conservative upper limits on surface temperature and luminosity; we therefore use this method throughout this work.*

We next fitted the *Chandra* data to a composite model that included the power-law component just discussed plus a hydrogen-atmosphere spectral model; the calculation of these atmospheric models is described in Appendix A. Our models are similar to those used routinely to model the spectra of quiescent neutron stars (e.g., Zavlin, Pavlov, & Shibano 1996; Rutledge et al. 1999). However, we extend our models to much larger values of mass and radius, and we also consistently include the effects of self-irradiation. Using the theory and methods detailed in Appendix A and adopting  $M(J1118) = 8 M_\odot$  (§1), we computed a grid of spectra on each of nine different surfaces with radii relative to the Schwarzschild radius  $R_{\text{S}}$  ranging from  $\log R/R_{\text{S}} = 0.05$  to 0.45 in equal logarithmic steps of 0.05. Our smallest radius corresponds to the Buchdahl limit of  $R_{\text{min}} = 9/8 R_{\text{S}}$ , which is the minimum allowable radius for a stable star in general relativity (Buchdahl 1959; Weinberg 1972). At each radius, we computed 25 photon spectra ( $E = 0.01$ –10.0 keV) which correspond to temperatures of  $\log T_\infty = 5.00, 5.01, 5.02, \dots, 5.25$ , where the temperature at infinity  $T_\infty$  is related to the effective temperature at the surface of the star by  $T_\infty = T_{\text{eff}}/(1 + z)$ . The models were cast in the form of nine one-parameter ( $T_\infty$ ) FITS table models, one for each radius, using a Fortran program (onepar.f) that was kindly provided by Keith Arnaud. The table models so derived were used within XSPEC (Arnaud & Dorman 2003) to model a hydrogen atmosphere for the range of radii and temperatures described above.

At each radius, we determined an upper limit on  $T_\infty$  of a thermal component as follows. We first fitted the 12-channel pulse-height spectrum using Gehrels’ weighting to a model that includes interstellar absorption and a simple power-law component. In this case, however, we fixed the column depth at its estimated maximum value of  $N_{\text{H}} = 1.6 \times 10^{20} \text{ cm}^{-2}$  (§2) in order to obtain the most conservative (i.e., largest) upper limits on  $T_\infty$  and  $L_{\infty, \text{th}}$

(the thermal component of luminosity as measured at infinity). In this way we obtained  $\Gamma(\text{Gehrels}) = 1.97 \pm 0.24$  with a flux at 1 keV =  $(1.70 \pm 0.55) \times 10^{-6}$  ph keV $^{-1}$  cm $^{-2}$  s $^{-1}$  ( $\chi^2_\nu = 0.47$  for 10 dof).

We next created a composite source model by fixing the power-law component using the just-mentioned values of  $\Gamma$  and  $N_{\text{H}}$  and by adding in turn each of the nine atmospheric models. Since the normalization of the thermal component is determined by the source radius  $R$  and distance  $D = 1.8$  kpc, there remains only a single free parameter,  $T_\infty$ . Accordingly, we determined a 99% confidence level upper limit on  $T_\infty$  by successively increasing its value until the total  $\chi^2$  increased by 6.63 (Lampton, Margon, & Bowyer 1976).

## 4. Results

### 4.1. Limits on Temperature and Luminosity

We determined upper limits at the 99% confidence level on  $T_\infty$  by the method described in §3; these limits are given for each of the nine H-atmosphere models in column 7 of Table 1. Columns 2 through 6 give the radius, surface redshift, critical cosine  $\mu_c$  (defined in Appendix A),  $\log g$  (surface gravity), and  $\log T_{\text{eff}}$  for each model. The limits on  $T_\infty$  are shown plotted vs. radius in Figure 1 (filled circles). The highest temperature limits occur for Models 3 and 4 with  $R \approx 1.4 - 1.6 R_{\text{S}}$ :  $T_\infty \leq 126, 200$  K. We emphasize that these are strong limits on  $T_\infty$  for two reasons: First, in fitting the data we have adopted the Gehrels' weighting function which gives larger errors and hence more conservative limits than the conventional weighting function (§3). And second, these limits are based on the estimated maximum allowable value of the interstellar column density,  $N_{\text{H}} = 1.6 \times 10^{20}$  cm $^{-2}$  (§2). Furthermore, as illustrated in Figure 1, the temperature limits depend only weakly on  $N_{\text{H}}$  because the ISM is optically thin even at the lowest energies (§1).

Note that the effective temperature as measured at the surface,  $T_{\text{eff}}$  (Table 1, column 6), varies inversely with radius, reaching a maximum at the Buchdahl limit:  $R = 9/8 R_{\text{S}}$ . Columns 8 and 9 give upper limits on the luminosities at infinity  $L_{\infty, \text{th}}$  and at the surface of the star  $L_{\text{R}}$ , respectively, where  $L_{\text{R}} = 4\pi R^2 \sigma T_{\text{eff}}^4$  and  $L_{\infty, \text{th}} = L_{\text{R}} / (1 + z)^2$ ; these limits are plotted in Figure 2. The limiting value of  $L_{\infty, \text{th}}$ , which is of most interest, varies by only  $\approx 40\%$  over the range of radii considered; it reaches a maximum value for the most compact configuration, namely Model 1:  $L_{\infty, \text{th}} < 9.4 \times 10^{30}$  erg s $^{-1}$  (99% confidence level).

Because the compact objects modeled here are relatively large and cool, it might be thought that useful limits could also be achieved through observations in the UV. However, as shown in Figure 3, this is not possible. The figure shows the relationship of six atmospheric

models to a multiwavelength spectrum of J1118, which was published previously (MNG03). The models shown completely bracket the ranges of temperatures and radii considered in the text and in Table 1. The heavy horizontal line on the right is the best-fit model X-ray spectrum and indicates that *Chandra* is capable of detecting the surface emission for  $\log T_\infty = 5.15$ , but not for the cooler models with  $\log T_\infty = 5.05$ , as expected given the temperature limits summarized in Table 1. On the left of the plot is shown the UV/optical spectrum. Of most interest here is the HST FUV spectrum, which is centered at  $\nu \sim 2 \times 10^{15}$  Hz, and plunges downward to  $\log \nu F_\nu \sim -14.1$ . These data were obtained in a 14 ks observation with STIS using the G140L grating. A hard limit on the sensitivity of this observation is indicated by the upward arrow. The models in question are all much fainter than the UV limit indicated. We conclude that HST cannot provide useful constraints on the models. We also conclude that the observed UV/optical emission cannot be due entirely or in part to thermal emission from the surface of the compact object. For a discussion of the origin of the UV/optical emission, see MNG03.

## 4.2. Comparison with the Predominantly Thermal Spectra of Neutron Stars

The spectrum of J1118, with its absence of a thermal component, contrasts sharply with the 0.5–10 keV spectra of quiescent NS LMXBs. A soft thermal component is dominant (i.e., comprises  $\gtrsim 50\%$  of the total flux) in the 0.5–10 keV band in nearly all NS spectra, although a fainter power-law component is also often present. When the thermal component is fitted with a NS H-atmosphere (NSA) model, the derived temperatures are in the range  $kT_\infty = 0.05 - 0.3$  keV ( $\log T_\infty = 5.8-6.5$ ) and the source radii are consistent with surface emission from a NS with a  $\sim 10$  km radius. The following ten accreting NSs are known to have such a dominant, soft emission component: 47 Tuc X5 and X7 (Heinke et al. 2003a); Cen X-4 (Campana et al. 2000; Rutledge et al. 2001a); 4U 1608-52 (Asai et al. 1996); MXB 1659-29 (Wijnands et al. 2003bc); RX J170930.2-263927 (Jonker et al. 2003a); KS 1731-260 (Wijnands et al. 2001; Wijnands et al. 2002); X1745-203 (NGC 6440 CX1; in't Zand 2001); Aql X-1 (Rutledge et al. 2001b); and 4U 2129+47 (Nowak, Heinz, & Begelman 2002).

For two other NSs, EXO 1745-248 and SAX J1810.8-2609, the thermal component is less apparent, but it may well be present. For the latter source, Jonker, Wijnands, & van der Klis (2003b) found that their *Chandra* data are well-fitted by a simple power-law model with  $N_{\text{H}} = 3.3 \times 10^{21}$  cm $^{-2}$  and that the NSA and other one-component thermal models provided much poorer fits. However, when they fitted their data with an NSA plus power-law model, the reduced  $\chi^2$  decreased further (from 0.80 to 0.65 for 10 dof), and the inferred properties

Table 1. Upper Limits<sup>a</sup> on Temperature and Luminosity<sup>b</sup>

Model	$\log R/R_S$	$1 + z$	$\mu_c$	$\log g$	$\log T_{\text{eff}}$	$\log T_\infty$	$\log L_{\infty,\text{th}}$	$\log L_R$
1	0.0512	3.000	0.6383	14.654	5.557	5.080	30.974	31.928
2	0.10	2.205	0.3522	14.423	5.436	5.092	30.855	31.541
3	0.15	1.851	0.1094	14.246	5.367	5.100	30.833	31.368
4	0.20	1.646	0.0	14.096	5.317	5.101	30.836	31.269
5	0.25	1.512	0.0	13.959	5.277	5.098	30.848	31.207
6	0.30	1.416	0.0	13.830	5.243	5.092	30.868	31.170
7	0.35	1.344	0.0	13.708	5.213	5.084	30.893	31.150
8	0.40	1.289	0.0	13.589	5.186	5.075	30.922	31.142
9	0.45	1.245	0.0	13.474	5.161	5.066	30.953	31.144

Note. — All quantities are in cgs units.

<sup>a</sup> Limits are at the 99% level of confidence and based conservatively on a column density of  $N_{\text{H}} = 1.6 \times 10^{20} \text{ cm}^{-2}$  (§2) and Gehrels’ weighting (§3).

<sup>b</sup> Legend:  $R$ , stellar radius,  $R_S$ , Schwarzschild radius,  $z$ , surface redshift,  $\mu_c$ , cosine of critical angle,  $g$ , surface gravity,  $T_{\text{eff}}$ , effective temperature at stellar surface,  $T_\infty$ , temperature at infinity,  $L_{\infty,\text{th}}$ , thermal component of luminosity at infinity,  $L_R$ , luminosity at stellar surface.

of the thermal component were typical of the canonical systems listed above:  $kT_\infty \approx 0.07$  keV with the thermal component contributing about half of the unabsorbed flux. For EXO 1745–248 in Terzan 5, the *Chandra* ACIS-S data can be fitted by a simple power-law model; furthermore, the fitted value of the very large column density,  $N_{\text{H}} = 1.3 \times 10^{22} \text{ cm}^{-2}$ , agrees with an independent estimate (Wijnands et al. 2003a). However, the authors conclude that a thermal component of emission may contribute as much as 10% of the total emission (0.5–10 keV) with an NSA temperature as high as  $kT_\infty = 0.10$  keV.

An instructive comparison object to consider is the millisecond X-ray pulsar SAX J1808.4-3658, which lacks a detectable soft component of emission and has a moderate column density,  $N_{\text{H}} = 1.3 \times 10^{21} \text{ cm}^{-2}$ . Its luminosity is only a factor of several times greater than the luminosity of J1118; furthermore, the limit on its bolometric thermal luminosity (Campana et al. 2002) is a factor of  $\approx 5$  less than the limits we have set on the thermal luminosity of J1118 (Fig. 2a). However, the *temperature limit* that can be placed on any hypothetical thermal component in J1118 is far more stringent because of its minimal interstellar column:  $N_{\text{H}} = 1.2 \times 10^{20} \text{ cm}^{-2}$  (see below).

In the case of SAX J1808.4-3658, Campana et al. (2002) conclude that a power-law fit alone can adequately describe their data. They set an upper limit on the flux of a hypothetical blackbody component that is  $< 7\%$  of the power-law flux in the 0.5–10 keV band for assumed blackbody temperatures in the range  $kT_\infty = 0.1 - 0.3$  keV (unabsorbed fluxes; 90% confidence). Our corresponding limit on the ratio of the unabsorbed fluxes in an 0.5–10 keV band) for J1118 is a factor  $\approx 12$  lower, namely, 0.6% for Model 4 (Table 1). It is also important to note that the  $< 7\%$  limit set for SAX J1808.4-3658 is based on a measurement of (at most) 17% of the bolometric flux for a  $kT = 0.10$  keV blackbody (83% of the flux is absorbed in the ISM). Furthermore, for slightly lower and quite realistic neutron-star surface temperatures (e.g.,  $kT_\infty = 0.05$  keV) the fraction of the flux that is observable becomes extremely small (2.1%). Thus, a soft but luminous thermal component may be present in SAX J1808.4-3658 that is masked by the ISM. On the other hand, for the order-of-magnitude lower column density of J1118, the ISM transmits 67% (31%) of the bolometric flux of a  $kT_\infty = 0.10$  (0.05) keV blackbody thereby making a cool thermal component far easier to detect; yet none is seen in J1118.

Dominant soft X-ray emission is also known for 18 other X-ray sources located in globular clusters that are thought to be quiescent LMXBs containing NSs (Heinke et al. 2003b). However, these objects have not been observed in outburst nor have they exhibited type I bursts; moreover, about half of these objects are very faint. Consequently, although these sources attest to the ubiquity of thermal surface emission from NSs, they are less instructive than the confirmed and well-studied NSs cited and discussed above.

In summary, for most NSs the thermal component is dominant; in a few examples the thermal component is weaker but still may contribute 7–10% of the total 0.5–10 keV flux. In all cases where the thermal component is detected, the NSA temperature is  $kT_\infty \sim 0.1$  keV. *We emphasize that the corresponding temperature limit on thermal emission from J1118 is incomparably stronger because of the source’s very low column density:  $\log T_\infty < 5.10$ ,  $kT_\infty < 0.011$  keV (Table 1).* This limit corresponds to a maximum thermal contribution in the 0.5–10 keV band of  $< 0.6\%$  (99% confidence level).

## 5. Discussion

We have seen in the previous sections that XTE J1118+480 in quiescence has no detectable component of thermal surface emission; a conservative 99% confidence level upper limit on the luminosity in such a component is  $L_{\infty,\text{th}} < 9.4 \times 10^{30}$  erg s<sup>−1</sup>. In comparison, quiescent NS LMXBs have significantly larger luminosities, typically  $L_{\infty,\text{th}} \sim \text{few} \times 10^{32}$  to  $\text{few} \times 10^{33}$  erg s<sup>−1</sup> (see references in §4.2). Before trying to interpret this difference, we need to decide what causes the surface emission in NS LMXBs. Two possibilities have been discussed in the literature: deep crustal heating, and accretion. Both require the accreting star to possess a surface. We discuss the two possibilities in the following two subsections.

### 5.1. Thermal Surface Emission from Deep Crustal Heating

Brown et al. (1998) showed that gas accreting onto the surface of a NS releases heat energy through nuclear reactions deep within the crust. These deep crustal reactions occur at a pressure of  $\sim 10^{30} - 10^{31}$  dyne cm<sup>−2</sup>. The diffusion time from this depth to the surface of the NS is on the order of 1 – 10 years, which is much longer than the typical duration of an accretion outburst in a transient LMXB. Therefore, the deep crustal heat energy escapes mostly during the quiescence phase of the systems and is expected to be observed as a steady thermal flux from the NS surface.

Brown et al. (1998) estimate that about 1.45 MeV of energy is released by the deep crustal reactions per accreted nucleon. Since the accretion luminosity is also proportional to the number of nucleons accreted, there is a direct proportionality between the fluence  $S_{\text{acc}}$  due to accretion and the fluence  $S_{\text{dch}}$  due to deep crustal heating:

$$S_{\text{acc}} = 135 \frac{\eta}{0.2} S_{\text{dch}}, \quad (1)$$

where  $\eta$  is the radiative efficiency of the accretion flow:  $L_{\text{acc}} = \eta \dot{M} c^2$ . Brown et al. (1998) show that the quiescent luminosity predicted from deep crustal heating agrees rather well

with the observed quiescent luminosities of NS LMXBs, though some systems like Cen X-4 (Rutledge et al. 2001a) and KS 1731–260 (Wijnands et al. 2001; Rutledge et al. 2002b) may be problematic.

Equation (1) above is general and is not necessarily restricted to a NS. It ought, therefore, to apply to J1118 if the object has a surface crust of normal matter. The total energy emitted by J1118 during its accretion outburst of 2000 is estimated to be  $S_{\text{acc}} \sim 1.6 \times 10^{43}$  erg. This estimate was computed using the 1.5–12 keV flux observed by the All-Sky Monitor aboard RXTE over the entire 2000 outburst ( $\approx 200$  days), and by approximating the source spectrum as a pure power law with photon index  $\Gamma = 1.78$  extending over the energy range 0.3–120 keV (McClintock et al. 2001b). The accretion efficiencies  $\eta$  of Models 1 to 9 described in §4 and Appendix A vary from 0.18 to 0.67, with a typical value of about 0.3. Using the latter value, we estimate that J1118 should, as a result of the 2000 outburst, have a net fluence of escaping deep crustal heat of order  $S_{\text{dch}} \sim 8 \times 10^{40}$  erg. The duration over which the heat escapes is given by the diffusion time from the layer where the reactions occur to the surface. For lack of a better estimate, we take the time to be  $\sim 1 - 10$  yr, as calculated by Brown et al. (1998) for NSs. We then predict a post-outburst quiescent thermal luminosity in J1118 of  $\sim 2.5 \times 10^{32} - 2.5 \times 10^{33}$  erg s $^{-1}$ . This is tens to hundreds of times larger than the conservative 99% confidence level upper limit we have derived from our observations.

An alternative approach is to consider the time averaged accretion rate of J1118 (rather than the mass accreted during the last outburst) and to estimate thereby the mean deep crustal heating rate. For a slightly evolved secondary and a binary with an orbital period of 4.1 hr, King, Kolb, & Burderi (1996) estimate the mass transfer rate from the secondary to be  $\sim 10^{-10}$  M $_{\odot}$ yr $^{-1}$ . Assuming that most of the transferred mass ultimately accretes onto the compact star, this gives a mean deep crustal heating rate of  $9 \times 10^{33}$  erg s $^{-1}$ , which is  $\approx 1000$  times larger than our upper limit on the quiescent thermal flux from J1118.

Both the above calculations indicate that J1118 is anomalously dim in quiescence compared to straightforward applications of the deep crustal heating model. One might be able to contrive a version of the model that brings the model predictions below the observed luminosity limit. Parameters that one could play with are the conductivity of the crust and the diffusion time from the heating layer to the surface. An exploration of these possibilities is beyond the scope of this paper. Colpi et al. (2001) invoked enhanced neutrino cooling in the core of the neutron star in Cen X-4 to explain the relatively low luminosity in quiescence of that source. A similar explanation, but with more extreme parameters, might work for J1118. This is worth exploring in more detail.

In our opinion, the most straightforward explanation of the observations is that J1118 simply does not generate any deep crustal heat through nuclear reactions. Since the reactions

invoked by Brown et al. (1998) are unavoidable in normal matter (but see §5.3 below), we suggest that J1118 is a true BH with an event horizon. The object has no surface, and hence no opportunity either to undergo deep crustal nuclear reactions or to radiate the released energy.

## 5.2. Thermal Surface Emission from Accretion

As discussed in §4.2, the spectra of quiescent NS LMXBs show two distinct components, a thermal component and a power-law component, with the former typically having a somewhat larger flux by a factor of a few. The most natural explanation for the power-law component is accretion, since there is no reasonable scenario in which deep crustal heating or any other energy source inside the NS will lead to power-law emission. We consider in this subsection the possibility that even the thermal component is the result of accretion (e.g., Narayan et al. 1997b). This is a reasonable hypothesis for several reasons. First, if the power-law emission arises close to the surface of the NS, then a good fraction of the radiation will impinge on the surface of the star and will be thermalized and re-emitted as a soft thermal component. Second, several models of accretion onto a NS show that a fraction of the accretion energy is released below the photosphere, leading to spectra that consist of both a thermal and a power-law component (Shapiro & Salpeter 1975; Turolla et al. 1994; Zampieri et al. 1995; Zane, Turolla, & Treves 1998; Deufel, Dullemond & Spruit 2001). Finally, the fact that the thermal component varies significantly in some sources (Rutledge et al. 2002a) is natural in an accretion model but very problematic with the deep crustal heating model.

Since transient BH LMXBs and NS LMXBs are very similar in many respects, one might expect their luminosities in quiescence to be comparable. Indeed, Menou et al. (1999) showed that *Eddington-scaled* quiescent luminosities should be comparable for systems with similar orbital periods; equivalently, the *unscaled* luminosities of BH LMXBs should be larger by a factor of several (the ratio of BH mass to NS mass) than the luminosities of NS LMXBs. Quiescent BH LMXBs are, however, actually seen to be very much fainter than quiescent NS LMXBs. This was first pointed out by Narayan et al. (1997b) and later confirmed in other studies (Menou et al. 1999; Garcia et al. 2001; MNG03). Figure 4 shows the latest data, including new results from Tomsick et al. (2003a,b). We see that the Eddington-scaled luminosities of BH LMXBs are orders of magnitude less than those of NS LMXBs with comparable orbital periods. Figure 5 shows the same results without using the Eddington scaling. Even in this representation, it is clear that quiescent BH LMXBs are very much fainter than quiescent NS LMXBs, whereas they should be brighter according to the Menou

et al. (1999) scalings.

The large difference between BH LMXBs and NS LMXBs in quiescence is surprising because the two sets of sources are expected to have similar mass transfer rates and mass accretion rates (e.g., King et al. 1996 and the discussion in MNG03). One potential explanation for the difference is that BH LMXBs radiate most of their emission in a thermal component and that this component is much cooler than in NS LMXBs because of the larger surface area of BH candidates. The thermal component in a BH candidate might then be so cool that it is heavily absorbed by the ISM, leading to a spuriously low estimate of the luminosity of the system.

The above hypothesis can be tested with J1118 since the source has an extraordinarily low interstellar column, so that even a very cool thermal component can, in principle, be detected. Combining the 99% confidence level upper limit on the thermal component of  $9.4 \times 10^{30}$  erg s<sup>-1</sup> derived in §4.1, with the power-law luminosity of  $3.5 \times 10^{30}$  erg s<sup>-1</sup> reported in MNG03, we derive an upper limit of  $1.3 \times 10^{31}$  erg s<sup>-1</sup> for the total quiescent luminosity of J1118. This limit is shown in Figures 4 and 5 as a filled square. Even after allowing for the maximum amount of soft thermal emission that J1118 can possibly have, we see that the quiescent luminosity of this source is still very much less than that of comparable NS LMXBs.

The large difference between BH LMXBs and NS LMXBs in quiescence finds a natural explanation if BHs have event horizons. Narayan et al. (1997b) proposed that (i) accretion in quiescent LMXBs occurs via an advection-dominated accretion flow (ADAF; Narayan & Yi 1994, 1995; Abramowicz et al. 1995; Narayan, Mahadevan & Quataert 1998), for which there is considerable supporting evidence (Narayan, McClintock & Yi 1996; Narayan, Barret & McClintock 1997a; Esin, McClintock & Narayan 1997; Esin et al. 1998, 2001), and (ii) that BH LMXBs are unusually dim because they advect most of the accretion energy into the BH through the event horizon, in contrast to NS LMXBs which radiate the advected energy from the surface of the NS. According to this model, the difference in luminosity between quiescent BH LMXBs and NS LMXBs is a direct consequence of the fact that BH candidates have event horizons whereas NSs have surfaces.

Several authors have proposed astrophysically motivated counter-explanations for the data shown in Figures 4 and 5 (Bildsten & Rutledge 2000; Stella et al. 2000; Nayakshin & Svensson 2001; Fender, Gallo & Jonker 2003), but many of these proposals have encountered difficulties as a result of later observations (see Narayan et al. 2002 and Kong et al. 2002).

### 5.3. Exotic Physics

The previous two subsections show that, within the realm of astrophysically reasonable explanations, it is hard to understand (i) the lack of a thermal component in the spectrum of J1118, and more generally, (ii) the low luminosity in quiescence of the source. The most reasonable explanation is that the object is a black hole. We also note the argument of Narayan & Heyl (2002), according to which the absence of Type I X-ray burst from J1118 argues against the presence of a surface. Here we investigate models based on exotic physics to see if any of these are consistent with the observations. The literature on exotic models is vast, and we are able to deal with only a small fraction of it here.

Glendenning (2000), Haensel (2004) and Weber (2004) discuss several exotic alternatives to the traditional neutron star, including relatively minor modifications such as a neutron star with a pion or kaon core as well as other more extreme possibilities such as hyperon stars, quark-hybrid stars, strange stars, etc. Most of these alternatives give viable models only for stellar masses  $\lesssim 2-3M_{\odot}$  and are not relevant for J1118 or other black hole candidates, which are more massive. Nevertheless, one might wish to consider whether such models would be consistent with the data on J1118 if they could somehow survive at a mass  $\sim 8M_{\odot}$ .

Bodmer (1971) and Witten (1984) suggested that the true ground state of the strong interaction may not be  $^{56}\text{Fe}$ , but a state of deconfined quark matter in a color superconducting state. If this is the case, it would be possible to have a “strange star” that is made largely of such quark matter (e.g., Dey et al. 1998). Such stars tend to be more compact than neutron stars (though still respecting the Buchdahl limit,  $R < 9/8R_S$ ). The maximum mass of these models is  $< 3M_{\odot}$  (Glendenning 2000; Haensel 2004; Prasad & Bhalerao 2004), so they are usually considered as an alternative to neutron stars and not as a model of a black hole candidate like J1118. In addition, when one of these stars accretes gas, it develops a surface crust of normal matter (e.g., Usov 1997; Zdunik 2002; Weber 2004) that floats above the quark substrate because of a repulsive Coulomb barrier. The crust extends down to a density of order the neutron drip point ( $\sim 10^{12} \text{ g cm}^{-3}$ ), and is indistinguishable from the crust of a normal neutron star. Consequently, the star will undergo deep crustal heating reactions (§5.1) and Type I X-ray bursts (Narayan & Heyl 2002), and will release accretion energy in the form of X-rays (§5.2), just as in the standard model. (See Sinha et al. 2002 for a discussion of possible burst characteristics of strange quark stars.) Therefore, even if the model could be extended to the mass range of black hole candidates (which is unlikely, see Glendenning 2000; Weber 2004), it could still be ruled out for J1118.

Alford, Rajagopal & Wilczek (1999) showed that at asymptotically large densities, a color-flavor locked (CFL) state of up, down and strange quarks is favored over other forms of color superconducting quark matter. Compact stars made of CFL matter have been

considered by some authors. The maximum mass of the star appears to be about  $4.5M_{\odot}$  (Horvath & Lugones 2004), which is too low for most black hole candidates. If the CFL phase is not the global energy minimum state at zero pressure, then a CFL star would consist of CFL matter in the core and normal matter in the crust (e.g., Alford et al. 2001). Such a model can be ruled out by the arguments presented in §§5.1, 5.2. However, if the CFL matter is the true ground state at zero pressure, then it is possible to have a bare CFL star.

In contrast to the strange star discussed earlier, a bare CFL star has no electrical charge and therefore does not support a crust electrostatically. Thus, one could visualize a situation in which accreting gas is immediately converted to CFL matter on contact with the surface of the star. Since no baryons or nuclei survive, there will be no deep crustal heat generation (or Type I X-ray bursts, Abramowicz, Kluzniak & Lasota 2002). Moreover, CFL matter is a very poor emitter of electromagnetic radiation at keV temperatures (Jaikumar, Prakash & Schäfer 2002), so the star will be very dim. An object like this would be hard to rule out by means of observations (Horvath & Lugones 2004). Another variant is a CFL star with a crust made up of a two color-flavor superconductor (2SC) or some other phase of quark matter (Weber 2004). The second phase does have electric charge (including free electrons) and it is expected to be an efficient radiator of electromagnetic radiation (Page & Usov 2002). Yet other forms of quark matter and their possible relevance to compact stars are reviewed by Weber (2004), but we do not discuss them here.

In summary, the situation with respect to models based on the CFL phase is fairly uncertain. Certain types of CFL stars — the bare variety with CFL matter extending out to the surface — are indistinguishable from black holes, at least via electromagnetic signals. But more study of the CFL phase is needed before one can decide if these models are viable. In particular, it is important to determine if the CFL phase is the ground state of quark matter at zero pressure, and even if it is, whether models based on it can exist at masses approaching  $10M_{\odot}$ .

Some theories of the strong interaction allow nucleons to be confined at densities below nuclear density. Compact stars made of this so-called Q-matter have been considered by Bahcall, Lynn & Selipsky (1990) and Miller, Shahbaz & Nolan (1998). A feature of Q-stars is that their maximum mass can be quite high, in principle even above  $100M_{\odot}$  if the Q-phase can exist at sufficiently low density. These models are thus relevant for black hole candidates. There is very little discussion in the literature on what happens when gas accretes on a Q-star. Since Q-matter is made of normal baryons and electrons, accreting gas should form an electrostatically supported crust of normal matter, just as in the case of the (non-CFL) strange star discussed earlier. If this is the case, then a Q-star will have deep crustal reactions and Type I X-ray bursts, and will release accretion energy in the form of electromagnetic

radiation. The model can then be ruled out by the observations.

Moving on to more exotic possibilities, one could consider a two-component model of a compact star in which one of the components is ordinary gas and the other is a non-interacting form of dark matter. The dark matter, which dominates the mass, may be either fermionic or bosonic. Such models have been studied in the past (Lee & Pang 1987; Zhang 1988; Henriques, Liddle & Moorhouse 1989; Jin & Zhang 1989; Yuan, Narayan & Rees 2004). In a related class of models, the dark component may consist of shadow or mirror matter living in a different sector (Khlopov et al. 1989). A feature of all these models is that the gas component has radii, surface gravities and surface redshifts similar to those of a neutron star (Yuan et al. 2004). Thus, the objects are expected to behave like neutron stars when they accrete gas. Specifically, they ought to release a similar amount of heat through deep crustal reactions and should be as bright as neutron star systems at the same mass accretion rate. As the discussion in §§5.1, 5.2 indicates, J1118 behaves quite differently from a neutron star and thus is not consistent with any of these models.

Chapline et al. (2001) have proposed that the event horizon of a classical black hole corresponds to a quantum phase transition with properties similar to the critical point of a Bose fluid. In this interpretation, there is no true event horizon. Therefore, a black hole will radiate whatever energy accretes on it, and it is not expected that black hole X-ray binaries in quiescence should be anomalously dim compared to neutron star systems. However, the spectrum of the emitted radiation might be quite different from a simple blackbody (Barbieri, Chapline & Santiago 2003). It would be of interest to calculate the spectrum of a stellar-mass quantum black hole in a quiescent X-ray binary to check whether the model is consistent with the observations shown in Figures 4 and 5.

Robertson and Leiter (2002, 2003) have used a new class of solutions of the Einstein field equations of general relativity to describe black hole candidates as magnetospheric, eternally-collapsing objects (MECO) that have a surface redshift  $z \sim 10^8$ . The magnetic field is assumed to be anchored and corotating with the central object. The predicted magnetic spindown luminosity and spectrum of the power-law component in quiescence is consistent with the observed values for J1118 (§1) for an intrinsic magnetic moment of  $\sim 3.4 \times 10^{29}$  G cm<sup>3</sup>, assuming that the dipole is aligned along the spin axis and spinning slowly at  $\sim 8$  Hz (D. Leiter, private communication). Our limits on the temperature and luminosity of the thermal component of J1118 (§4.1) can be accommodated if the surface redshift of the object exceeds  $1.39 \times 10^8$  (eqn. 17 in Robertson and Leiter 2003).

Finally, Abramowicz et al. (2002) invoked the gravitational condensate star model (or gravastar model) of Mazur & Mottola (2002) and argued that there is no way to distinguish such an object, which has a surface at a radius  $R$  only slightly greater than  $R_S$ , from a genuine

black hole with an event horizon. They make this claim based on the surface redshift, which is very large (because  $R$  is close to  $R_S$ ). However, if the source is in steady state and the luminosity is the result of accretion, then, regardless of the surface redshift, the binding energy of the accreting gas has to be radiated to infinity. In fact, the more compact the star, the larger the amount of binding energy released per unit accreted rest mass, and the larger the luminosity at infinity for a given mass accretion rate! Thus, the Abramowicz et al. argument is not valid for our problem; that is, the luminosity at infinity does *not* decrease as the surface redshift increases. However, we should note that the luminosity might come out in a form other than electromagnetic radiation, e.g., neutrinos or some kind of exotic particles (since the radiating gas can be very hot). Clearly, such models cannot be ruled out by the present work.

We should note that the gravitational condensate star is able to violate the Buchdahl limit,  $R \geq 9/8R_S$ , only because it invokes a negative-pressure interior (filled with vacuum energy,  $p = -\rho$ ). It also has an anomalously low entropy (Abramowicz et al. 2002). These features are unpalatable to many physicists.

## 6. Conclusions

We have examined the possibility that the dynamical black-hole candidate J1118 possesses a material surface rather than an event horizon. Either accretion onto such a surface or deep crustal heating would be expected to produce a quiescent thermal component of emission like those commonly observed for neutron stars. We have fitted our Chandra spectrum of J1118 to a model consisting of a fixed power-law component plus an atmospheric thermal component with variable temperature,  $T_\infty$ . The spectral fits were repeated for a series of nine atmospheric models with radii ranging from the minimum allowable,  $9/8 R_S$ , to a maximum of  $2.8 R_S$ . For the most compact of these models, which lie within their own photon spheres, the self-irradiation of the atmospheres was taken into account. No emission in excess of a simple power-law component was detected in J1118, and very strong upper limits were set on the presence of a thermal source:  $kT_\infty < 0.011$  keV and  $L_{\infty,\text{th}} < 9.4 \times 10^{30}$  erg s<sup>-1</sup> (99% confidence level).

If one assumes that the hypothetical crust of J1118 is composed of normal nuclear matter, then this stringent limit on a thermal component of luminosity is hard to reconcile with the theory of deep crustal heating and the observed fluence of J1118 during its outburst in 2000: The predicted quiescent luminosity exceeds the above limit on  $L_{\infty,\text{th}}$  by a factor of  $\gtrsim 25$ . Possibly a contrived model of deep crustal heating and/or an extreme model of neutrino cooling of the core could explain this difference. On the other hand, if J1118

possesses a material surface and accretion powers the thermal emission seen from NSs, then one expects J1118 to have a luminosity at least as great as that of an average NS, whereas its *total* luminosity in Eddington-scaled units is about 100 times less than the luminosity of a typical NS and fully 10 times less than the luminosity of even SAX J1808.4-3658 (Fig. 4).

The above limit on thermal emission, in combination with the observed power-law emission, yields a very tight limit on the *total* quiescent luminosity of  $1.3 \times 10^{31}$  erg s<sup>-1</sup>, which is far below the luminosities observed for NSs. Because of the high transparency of the ISM, our results rule out the possibility that the total luminosity of J1118 could be augmented significantly by any ultrasoft component of emission. Thus J1118 – and by inference the other dynamical BH candidates – are truly faint relative to NSs (Figs. 4 and 5).

In summary, a sensitive search has failed to detect any thermal emission from a hypothetical surface surrounding J1118, although NSs very commonly show such surface emission due to either deep crustal heating or accretion. Our sensitivity to a thermal component of emission from J1118 is much greater than the emission predicted by the theory of deep crustal heating, assuming that J1118 has a material surface analogous to that of NSs. Likewise, there is no evidence that accretion is occurring in quiescence onto the surface of J1118, which is the mechanism often invoked to explain the far greater thermal luminosities of NSs. The simplest explanation for the absence of any thermal emission is that J1118 lacks a material surface and possesses an event horizon.

Finally, our limits on thermal emission from J1118 rule out the possibility that there is a heretofore unseen and appreciable soft component of luminosity. This result implies that the dynamical BH candidates are truly faint relative to NSs and underscores our original argument that these compact objects have event horizons and are therefore genuine black holes (Narayan et al. 1997b). As discussed in §5.3, however, we cannot at this time rule out certain very exotic alternatives.

### A. Atmospheric Models

The emergent spectra of the compact objects specified in the previous section are found by modeling their atmospheres. Our approach is similar to the modeling done by Zavlin et al. (1996), except for certain modifications due to self-irradiation of the atmosphere when the surface of the object is inside its own photon sphere.

The atmospheric models used here incorporate relatively simple physics, in keeping with the purpose of the paper to provide bounds, rather than detailed spectral comparisons. The major assumptions are:

1. Negligible magnetic field.
2. Spherical object with static, plane-parallel atmosphere in radiative equilibrium.
3. Ideal equation of state for pure hydrogen with complete ionization.
4. Opacity due to free-free absorption plus Thomson scattering in the unpolarized, isotropic approximation.

A few comments on the above assumptions: Negligible magnetic field  $B$  in this context implies  $B \ll 10^8\text{--}10^{10}$  G (Zavlin et al. 1996). The scale heights in the atmosphere are much less than the radius, so the plane-parallel assumption is a good one. The assumption of pure hydrogen is appropriate for a slowly accreting object with sufficient time for gravitational settling. Within the zones where ideal behavior is valid, complete ionization is a good assumption at the highest effective temperatures ( $\sim 10^6$  K) considered, but will be less good at the lowest ( $\sim 10^5$  K). The complete ionization assumption implies that bound-free and bound-bound opacities need not be included. As indicated above, this is less valid for the lowest temperatures considered. However, even there the bound-free and bound-bound features are still well below the peak of the spectrum, and would probably have only a minor effect on our conclusions.

We shall now describe the relevant general relativistic effects, followed by our results for the atmospheric modeling.

### A.1. General Relativistic Effects

Schwarzschild geometry exactly describes the region outside the spherical star, and is also applicable to a high degree of approximation within the thin atmosphere. Here we review aspects of Schwarzschild geometry relevant to the present discussion only briefly, referring to discussions in standard texts, especially Misner, Thorne & Wheeler (1973, hereafter MTW). Using standard notation (MTW, p. 655), the metric in Schwarzschild coordinates is,

$$ds^2 = -(1 - R_S/r) dt^2 + (1 - R_S/r)^{-1} dr^2 + r^2 (d\theta^2 + \sin^2 \theta d\phi^2); \quad R_S = 2GM/c^2. \quad (\text{A1})$$

It follows that the gravitational redshift and time dilation are given in terms of the redshift factor

$$1 + z = (1 - R_S/r)^{-1/2}. \quad (\text{A2})$$

In particular, a photon of frequency  $\nu$  at the surface radius  $r$  will be observed at frequency  $\nu_{\text{obs}} = (1 + z)^{-1}\nu$  at large radius  $r_{\text{obs}}$ ,  $r_{\text{obs}} \gg R_S$ . Likewise a time interval  $dt$  at the surface

will appear as  $dt_{\text{obs}} = (1 + z) dt$  at  $r_{\text{obs}}$ . One notes that the product  $dt d\nu = dt_{\text{obs}} d\nu_{\text{obs}}$  is therefore an invariant.

It is important to determine how the photon flux observed at a large radius  $r_{\text{obs}}$  is related to the flux at the surface radius  $r$ . [In this Appendix,  $r$  is used to denote both a general radius and also the radius of the object, called  $R$  in the main body of the paper.] One notes that in steady state the same number of photons  $dN$  flowing out from the surface in a time interval  $dt$  will pass through the spherical surface at  $r_{\text{obs}}$  in time interval  $dt_{\text{obs}}$ . Since the area of a spherical surface in Schwarzschild geometry is simply proportional to the square of the Schwarzschild radial coordinate, this implies that the photon flux expressed as number of photons per area per time per frequency interval transforms in the following way:

$$\left( \frac{dN}{dA dt d\nu} \right)_{\text{obs}} = \frac{r^2}{r_{\text{obs}}^2} \left( \frac{dN}{dA dt d\nu} \right)_{\text{surface}}. \quad (\text{A3})$$

Often it is more convenient to use a flux based on photon energy,  $F = dE/dA dt d\nu$ . Since  $dE = h\nu dN$ , this implies the transformation of flux,

$$F(r_{\text{obs}}, \nu_{\text{obs}}) = (1 + z)^{-1} \frac{r^2}{r_{\text{obs}}^2} F[r, (1 + z)\nu_{\text{obs}}]. \quad (\text{A4})$$

The surface flux  $F(r, \nu)$  is found by atmospheric modeling. The observed flux  $F(r_{\text{obs}}, \nu_{\text{obs}})$  can then be determined using equation (A4). The transformations of other quantities related to flux can be found in similar fashion.

As an instructive example, consider the special case where the surface emits as a black-body of temperature  $T_{\text{eff}}$ . The surface flux is then given in terms of the Planck function  $B(\nu, T)$ ,

$$F(r, \nu) = \pi B(\nu, T_{\text{eff}}) = \pi \frac{2h\nu^3/c^2}{\exp(h\nu/kT_{\text{eff}}) - 1}. \quad (\text{A5})$$

Substitution of this into Eq. (A4) gives,

$$F(r_{\text{obs}}, \nu_{\text{obs}}) = (1 + z)^2 \frac{r^2}{r_{\text{obs}}^2} \pi B(\nu_{\text{obs}}, T_{\infty}), \quad (\text{A6})$$

where,

$$T_{\infty} = \frac{T_{\text{eff}}}{1 + z}. \quad (\text{A7})$$

Although this is a very special case, the form of Eq. (A6) suggests that in general  $T_{\infty}$  may better characterize the shape of the observed spectrum than  $T_{\text{eff}}$ . Accordingly, we shall use  $T_{\infty}$  to parameterize our models.

So far we have considered the *global* consequences of general relativity, those determining the relationship between local quantities at the surface of the object with observed quantities at large distance. We now shall consider what *local* consequences there might be on the structure of the atmosphere itself.

To the extent that the atmosphere depends only on local variables, such as effective temperature and gravity, one can consider the atmospheric modeling problem as identical to the “standard” one by moving into the local proper frame of the atmosphere. Since the chemical composition is fixed here (pure ionized hydrogen), we shall regard the two local quantities  $T_{\text{eff}}$  and  $g$  as constituting the complete parameterization of the atmosphere. If the mass and radius of the object are given, then  $g$  is given in Schwarzschild geometry by the corrected Newtonian formula,

$$g = (1 + z) \frac{GM}{r^2}, \quad (\text{A8})$$

for an object of mass  $M$  and radius  $r$  (Zeldovich & Novikov 1971, Eq. (3.2.3), p. 87). The above simple local picture is valid as long as the radius  $r$  of the atmosphere lies outside the photon orbit corresponding to mass  $M$ , i.e., the radius satisfies  $r > (3/2)R_S$ . In this case all surface rays emergent in the outward hemisphere escape to infinity, although they may suffer gravitational bending. Conversely, all rays in the inward hemisphere come from infinity and have zero intensity. In the language of stellar atmospheres, the boundary condition on the intensities at the surface is

$$I(r, \nu, -\mu) = 0, \quad 0 \leq \mu \leq 1, \quad (\text{A9})$$

where  $\mu = \cos \theta$  and  $\theta$  is the angle between the ray and the outward normal. This is the standard boundary condition, so the construction of the atmosphere is “standard” in every sense.

However, when  $r < (3/2)R_S$  the surface lies inside the *photon sphere*. In this case only those rays within a certain critical cone about the outward normal will escape, that is, for  $\theta < \theta_c$ , where [MTW, p. 675]

$$\sin \theta_c = \frac{3^{3/2}}{2} \left(1 - \frac{R_S}{r}\right)^{1/2} \frac{R_S}{r}. \quad (\text{A10})$$

Rays outside this critical cone,  $\theta > \theta_c$ , will be gravitationally bent enough to cause them to return to the surface, at the same angle, but now with respect to the inward normal. Thus a portion of the incoming radiation will have non-zero intensity, in fact the same intensity as the emergent rays for the corresponding angle. The boundary condition then becomes,

$$I(r, \nu, -\mu) = \begin{cases} 0, & \mu_c \leq \mu \leq 1, \\ I(r, \nu, \mu), & 0 \leq \mu \leq \mu_c \end{cases} \quad (\text{A11})$$

where

$$\mu_c = \cos \theta_c. \quad (\text{A12})$$

It is seen that the rays outside the critical cone are in effect specularly reflected (angle of incidence equals angle of reflection). This *self-irradiation* is a nonlocal effect of general relativity that does not have any analogy in the “standard” atmosphere problem.

The most compact object to be considered here is one at the Buchdahl limit  $(9/8)R_S$ , where the critical cosine is  $\mu_c = (11/27)^{1/2} = 0.6383\dots$ . Thus, there is potentially a reduction in the available solid angle for escaping rays by a factor of order two or more.

Given the unusual nature of the intensity field at the surface in the self-irradiation case, it is worthwhile to re-examine the definition of surface flux. We start with the formula for flux for an object with spherical symmetry,

$$F(r, \nu) = 2\pi \int_{-1}^1 I(r, \nu, \mu) \mu d\mu. \quad (\text{A13})$$

The effective temperature  $T_{\text{eff}}$  is defined using the total surface flux, which is found by integrating  $F(r, \nu)$  over frequencies,

$$\sigma T_{\text{eff}}^4 = \int_0^\infty F(r, \nu) d\nu, \quad (\text{A14})$$

where  $\sigma$  is the Stefan-Boltzmann constant. Equations (A13) and (A14) apply to all cases.

We shall now show how (A13) simplifies in the standard case and in the self-irradiation case. In the standard case,  $r > (3/2)R_S$ , the intensity vanishes for  $\mu < 0$  (cf. Eq. [A9]), so that equation (A13) can be written as an integral over the outward hemisphere alone,

$$F(r, \nu) = 2\pi \int_0^1 I(r, \nu, \mu) \mu d\mu, \quad r > (3/2)R_S. \quad (\text{A15})$$

In the self-irradiation case,  $r < (3/2)R_S$ , we break the range of integration in Eq. (A13) into four intervals:  $(-1, -\mu_c)$ ,  $(-\mu_c, 0)$ ,  $(0, \mu_c)$ , and  $(\mu_c, 1)$ . From equation (A11), it is seen that the integral over the first interval is zero, while the integrals over the second and third cancel due to the reflection condition and the odd factor  $\mu$ . Therefore, the flux can be written as an integral over the fourth interval alone,

$$F(r, \nu) = 2\pi \int_{\mu_c}^1 I(r, \nu, \mu) \mu d\mu, \quad r < (3/2)R_S, \quad (\text{A16})$$

In either case, (A15) or (A16), the integration involves only escaping rays, as one would expect intuitively. Here we adopt the convention that  $\mu_c = 0$  when  $r > (3/2)R_S$ , making equation (A16) generally valid.

## A.2. Calculation of the Atmospheric Models

A code was written to solve for the emergent spectrum of the atmosphere. This code uses fairly standard techniques of discretization in depth, frequency, and angle, along with an iterative linearization technique for the temperature correction. The linearization is only “partial,” in that the temperature dependences of the opacities on the temperature were not linearized, but rather updated after each iteration. The convergence rate was nevertheless quite adequate.

A novel feature of the code is its ability to treat self-irradiation, which required the incorporation of the modified surface boundary condition (A11). This also involved using separate quadrature for the angular ranges inside and outside the critical cone. It was found that, per hemisphere, 3 angles within the cone and 2 outside gave adequate results.

In order to check the code, we computed a standard case (no self-irradiation) with parameters  $\log T_{\text{eff}} = 5.9$  and  $g = 2.43 \times 10^{14} \text{ cm s}^{-2}$ , a case considered by Zavlin et al. (1996). Our emergent intensities at values of  $\mu = 0.1, 0.4, 0.7,$  and  $1.0$  were compared to theirs (the left side of their Figure 4) with virtually perfect agreement.

The emergent flux vs. frequency of standard models for  $\log T_{\text{eff}} = 6.0, 5.5,$  and  $5.0$  are plotted in Figure 6. These models are for  $\log g = 14.1$ , but the gravity dependence is not strong, and these curves apply fairly well to the other gravities considered here. Note in this figure the abscissa is  $\log(\nu/T_{\text{eff}})$  and the ordinate is  $\log(F_{\nu}/T_{\text{eff}}^3)$ . With these rescalings, the various “standard” models lie close to a universal curve, which we have fitted to the form,

$$\frac{F_{\nu}}{T_{\text{eff}}^3} = 2.23 \times 10^{-17} q^{2.5} \exp[-q^{0.55}], \quad (\text{A17})$$

where,

$$q = 1.62 \times 10^{-10} \frac{\nu}{T_{\text{eff}}}, \quad (\text{A18})$$

which does not contain  $g$ . All quantities are in cgs units. We give this approximation for those who may need a quick, convenient way to estimate such spectra without doing the detailed atmospheric modeling. However, for the main calculations of this paper, we computed each individual model using the full code.

The primary effect of self-irradiation is to limit the available solid angle for escaping photons at the surface, which has the secondary effect of forcing the temperatures within the atmosphere to rise for the same effective temperature, thereby acting very much like the well known backwarming effect for line blanketing in stellar atmosphere theory (see, e.g., Mihalas 1978). This is shown in Figure 7, where temperature vs. pressure (depth) is given for models each with  $\log g = 14.654$  and  $\log T_{\text{eff}} = 6.0$ , but for values of  $\mu_c = 0, 0.1094, 0.3522,$  and

0.6383. The first of these corresponds to a “standard” model, while the last corresponds to one with maximal self-irradiation (at the Buchdahl limit). The self-irradiated models are hotter than the standard one at all depths, but especially near the surface.

As shown in Figure 8, the main effect of self-irradiation is to soften the spectrum. There are two reasons for this. First, the escape cone for emergent radiation is narrowed, which lowers the flux at both low and high frequencies. Second, the temperatures near the surface affect mostly the lower frequencies where the free-free opacities are largest, while the temperatures at large depth affect mostly the higher frequencies. As we have seen, the surface temperature is raised more than those at large depth, which favors the lower frequencies. The net result of these two effects is to yield the softened spectra seen in Figure 8, but to keep the same total flux, as it must for the same effective temperature.

It is perhaps worthwhile to point out that the softening of the spectrum here relies strongly on the substantial frequency dependence of the free-free opacity, as indicated in the previous paragraph. In fact, we have done analogous calculations for a frequency independent opacity (gray opacity), and have found that in that case the spectrum actually *hardens*.

We thank Keith Arnaud for assistance in implementing table models in XSPEC and for other advice, Craig Heinke and Peter Jonker for helpful discussions on quiescent neutron stars, Harvey Tananbaum for comments on the manuscript, Mike Garcia for help with updating Figures 4 and 5, and an anonymous referee for constructive and stimulating comments. This work has made use of the information and tools available at the HEASARC Web site, operated by GSFC for NASA, and was supported in part by NASA grants NAG5-9930 and NAG5-10780, and NSF grant AST 0307433.

## REFERENCES

- Abramowicz, M. A., Chen, X., Kato, S., Lasota, J.-P., & Regev, O. 1995, *ApJ*, 438, L37
- Abramowicz, M. A., Kluzniak, W., & Lasota, J.-P. 2002, *A&A*, 396, L31
- Alford, M., Rajagopal, K., & Wilczek, F. 1999, *Nucl. Phys.*, B537, 443
- Alford, M., Rajagopal, K., Reddy, S., & Wilczek, F. 2001, *Phys. Rev. D*, 64, 074017
- Arnaud, K., & Dorman, B. 2003, *XSPEC: An X-ray Spectral Fitting Package, User's Guide for version 11.3* (Greenbelt: NASA)
- Asai, K., Dotani, T., Mitsuda, K., Hoshi, R., Vaughan, B., Tanaka, Y., & Inoue, H. 1996, *PASJ*, 48, 257
- Bahcall, S., Lynn, B. W., & Selipsky, S. L. 1990, *ApJ*, 362, 251
- Balucinska-Church, M., & McCammon, D. 1992, *ApJ*, 400, 699
- Barbieri, J., Chapline, G., & Santiago, D. I. 2003, *Mod. Phys. Lett. A*, 18, 2767
- Bildsten, L., & Rutledge, R. E. 2000, *ApJ*, 541, 908
- Bodmer, A. R. 1971, *Phys. Rev. D*, 4, 1601
- Brown, E. F., Bildsten, L., & Rutledge, R. E. 1998, *ApJ*, 504, L95
- Buchdahl, H. A. 1959, *Phys. Rev.* 116, 1027
- Campana, S., Stella, L., Mereghetti, S., & Cremonesi, D. 2000, *A&A*, 358, 583
- Campana, S., et al. 2002, *ApJ*, 575, L15
- Chapline, G., Hohlfeld, E., Laughlin, R.B., & Santiago, D. I. 2001, *Phil. Mag.*, 81, 235
- Chaty, S., Haswell, C. A., Malzac, J., Hynes, R. I., Shrader, C. R., & Cui, W. 2003, *MNRAS*, 346, 689
- Colpi, M., Geppert, U., Page, D., & Possenti, A. 2001, *ApJ*, 548, L175
- Deufel, B., Dullemond, C. P., & Spruit, H. C. 2001, *A&A*, 377, 955
- Dey, M., Bombaci, I., Dey, J., Ray, S., & Samanta, B. C. 1998, *Phys. Lett. B*, 438, 123
- Dickey, J. M., & Lockman, F. J. 1990, *ARA&A*, 28, 215

- Done, C., & Gierlinski, M. 2003, MNRAS, 342, 1041
- Dubus, G., Kim, R. S. J., Menou, K., Szkody, P. & Bowen, D. V. 2001, ApJ, 553, 307
- Esin, A. A., McClintock, J. E., Drake, J. J., Garcia, M. R., Haswell, C. A., Hynes, R. I., & Muno, M. P. 2001, ApJ, 555, 483
- Esin, A. A., McClintock, J. E., & Narayan, R. 1997, ApJ, 489, 865
- Esin, A. A., Narayan, R., Cui, W., Grove, J. E., & Zhang, S.-N. 1998, ApJ, 505, 854
- Fender, R. P., Gallo, E., & Jonker, P. G. 2003, MNRAS, 343, L99
- Frontera, F., Amati, L., Zdziarski, A. A., Belloni, T., Del Sordo, S., Masetti, N., Orlandini, M., & Palazzi, E. 2003, ApJ, 592, 1110
- Frontera, F., et al. 2001, ApJ, 561, 1006
- Garcia, M. R., McClintock, J. E., Narayan, R., Callanan, P., Barret, D., & Murray, S. S. 2001, ApJ, 553, L47
- Garmire, G. P., et al. 1992, in AIAA Space Program & Technologies Conference (Reston: AIAA), 8
- Gehrels, N. 1986, ApJ, 303, 336
- Glendenning, N. K. 2000, Compact Stars: Nuclear Physics, Particle Physics, and General Relativity (New York: Springer)
- Haensel, P. 2004, in Final Stages of Stellar Evolution, eds. J.-M. Hameury & C. Motch (astro-ph/0301073)
- Heinke, C. O., Grindlay, J. E., Lloyd, D. A., & Edmonds, P. D. 2003a, ApJ, 588, 452
- Heinke, C. O., Grindlay, J. E., Lugger, P. M., Cohn, H. N., Edmonds, P. D., Lloyd, D. A., & Cool, A. M. 2003b, ApJ, 598, 501
- Henriques, A. B., Liddle, A. R., & Moorhouse, R. G. 1989, Phys. Lett. B, 233, 99
- Horvath, J. E., & Lugones, G. 2004, A&A, submitted (astro-ph/0402349)
- Hynes, R. I., Mauche, C. W., Haswell, C. A., Shrader, C. R., Cui, W., & Chaty, S. 2000, ApJ, 539, L37

- in't Zand, J. J. M., van Kerkwijk, M. H., Pooley, D., Verbunt, F., Wijnands, R., & Lewin, W. H. G. 2001, *ApJ*, 563, L41
- Jaikumar, P., Prakash, M., & Schäfer, T. 2002, *Phys. Rev. D*, 66, 063003
- Jin, K., & Zhang, Y. 1989, *Phys. Lett. A*, 142, 79
- Jonker, P. G., Mendez, M., Nelemans, G., Wijnands, R., & van der Klis, M. 2003a, *MNRAS*, 341, 823
- Jonker, P. G., Wijnands, R., & van der Klis, M. 2003b, *MNRAS*, in press (astro-ph/0311560)
- Khlopov, M. Yu, Beskin, G. M., Bochkarev, N. G., Pustilnik, L. A., & Pustilnik, S. A. 1991, *Sov. Astron.*, 35, 21
- King, A. R., Kolb, U., & Burderi, L. 1996, *ApJ*, 464, L127
- Kong, A. K. H., McClintock, J. E., Garcia, M. R., Murray, S. S., & Barret, D. 2002, *ApJ*, 570, 277
- Lampton, M., Margon, B., & Bowyer, S. 1976, *ApJ*, 208, 177
- Lee, T. D., & Pang, Y. 1987, *Phys. Rev. D*, 35, 3678
- Lockman, F. J., Jahoda, K., & McCammon, D. 1986, *ApJ*, 302, 432
- Mazur, E., & Mottola, P. O. 2002, *APS Meeting*, I12.011
- McClintock, J. E., Garcia, M. R., Caldwell, N., Falco, E. E., Garnavich, P. M., & Zhao, P. 2001a, *ApJ*, 551, 147
- McClintock, J. E., et al. 2001b, *ApJ*, 555, 477
- McClintock, J. E., Narayan, R., Garcia, M. R., Orosz, J. A., Remillard, R. A., & Murray, S. S. 2003, *ApJ*, 593, 435 [MNG03]
- McClintock, J. E., & Remillard, R. A. 2004, to appear in *Compact Stellar X-ray Sources*, eds. W. H. G. Lewin & M. van der Klis (Cambridge: Cambridge Univ. Press) (astro-ph/0306213 v3)
- Menou, K., Esin, A. A., Narayan, R., Garcia, M. R., Lasota, J.-P., & McClintock, J. E. 1999, *ApJ*, 520, 276
- Mihalas, D. 1978, *Stellar Atmospheres* (San Francisco: Freeman)

- Miller, J. C., Shahbaz, T., & Nolan, L. A. 1998, MNRAS, 294, L25
- Misner, C.W., Thorne, K.S., & Wheeler, J.A. 1973, Gravitation (San Francisco: Freeman) [MTW]
- Narayan, R., Barret, D., & McClintock, J. E. 1997a, ApJ, 482, 448
- Narayan, R., Garcia, M. R., & McClintock, J. E. 1997b, ApJ, 478, L79
- Narayan, R., Garcia, M. R., & McClintock, J. E. 2002, in Proc. Ninth Marcel Grossmann Meeting: On Recent Developments in Theoretical and Experimental General Relativity, Gravitation and Relativistic Field Theories, eds V. Gurzadyan, R. Jantzen, & R. Ruffini (Singapore: World Scientific) p405 (astro-ph/0107387)
- Narayan, R., & Heyl, J. S. 2002, ApJ, 574, 139L
- Narayan, R., Mahadevan, R., & Quataert, E. 1998, in The Theory of Black Hole Accretion Discs, ed. M. A. Abramowicz, G. Bjornsson, & J. E. Pringle (Cambridge: Cambridge Univ. Press) p148
- Narayan, R., McClintock, J. E., & Yi, I. 1996, ApJ, 457, 821
- Narayan, R., & Yi, I. 1994, ApJ, 428, L13
- Narayan, R., & Yi, I. 1995, ApJ, 452, 710
- Nayakshin, S., & Svensson, R. 2001, ApJ, 551, L67
- Nowak, M. A., Heinz, S., & Begelman, M. C. 2002, ApJ, 573, 778
- Orosz, J., et al. 2004, in preparation
- Page, D., & Usov, V. V. 2002, Phys. Rev. Lett., 89, 131101
- Prasad, N., & Bhalerao, R. S. 2004, Phys. Rev. D, 69, 103001
- Robertson, S. L., & Leiter, D. J. 2002, ApJ, 565, 447
- Robertson, S. L., & Leiter, D. J. 2003, ApJ, 596, L203
- Rutledge, R. E., Bildsten, L., Brown, E. F., Pavlov, G. G., and Zavlin, V. E. 1999, ApJ, 514, 945
- Rutledge, R. E., Bildsten, L., Brown, E. F., Pavlov, G. G., & Zavlin, V. E. 2001a, ApJ, 551, 921

- Rutledge, R. E., Bildsten, L., Brown, E. F., Pavlov, G. G., & Zavlin, V. E. 2001b, *ApJ*, 559, 1054
- Rutledge, R. E., Bildsten, L., Brown, E. F., Pavlov, G. G., & Zavlin, V. E. 2002a, *ApJ*, 577, 346
- Rutledge, R., Bildsten, L., Brown, E. F., Pavlov, G. G., Zavlin, V. E., & Ushomirsky, G. 2002b, *ApJ*, 580, 413
- Shapiro, S. L., & Salpeter, E. E. 1975, *ApJ*, 198, 671
- Sinha, M., Dey, M., Ray, S., & Dey, J. 2002, *MNRAS*, 337, 1368
- Stella, L., Campana, S., Mereghetti, S., Ricci, D., & Israel, G. L. 2000, *ApJ*, 537, L115
- Sunyaev, R., & Revnivtsev, M. 2000, *A&A*, 358, 617
- Tomsick, J. A., et al. 2003a, *ApJ*, 597, L133
- Tomsick, J. A., Gelino, D. M., Halpern, J. P., & Kaaret, P. 2003b, *BAAS*, 203, #53.13
- Turolla, R., Zampieri, L., Colpi, M., & Treves, A. 1994, *ApJ*, 426, L35
- Usov, V. V. 1997, *ApJ*, 481, L107
- van Speybroeck, L. P., Jerius, D., Edgar, R. J., Gaetz, T. J., Zhao, P., & Reid, P. B. 1997, *Proc. SPIE*, 3113, 89
- Wagner, R. M., Foltz, C. B., Shahbaz, T., Casares, J., Charles, P. A., Starrfield, S. G., & Hewett, P. 2001, *ApJ*, 556, 42
- Weber, F. 2004, *Progress in Particle and Nuclear Physics*, in press (astro-ph/0407155)
- Weinberg, S. 1972, *Gravitation and Cosmology: Principles and Applications of the General Theory of Relativity* (New York: Wiley)
- Wijnands, R., Guainazzi, M., van der Klis, M., & Mendez, M. 2002, *ApJ*, 573, L45
- Wijnands, R., Heinke, C. O., Pooley, D., Edmonds, P. D., Lewin, W. H. G., Grindlay, J. E., Jonker, P. G., & Miller J. M. 2003a, submitted to *ApJ* (astro-ph/0310144)
- Wijnands, R., Homan, J., Miller, J. M., & Lewin, W. H. G. 2003b, submitted to *ApJ* (astro-ph/0310612)

- Wijnands, R., Miller, J. M., Markwardt, C., Lewin, W. H. G., & van der Klis, M. 2001, *ApJ*, 560, L159
- Wijnands, R., Nowak, M., Miller, J. M., Homan, J., Wachter, S., & Lewin, W. H. G. 2003c, *ApJ*, 594, 952
- Witten, E. 1984, *Phys. Rev. D*, 30, 272
- Yuan, Y.-F., Narayan, R., & Rees, M. J. 2004, *ApJ*, 606, 1112
- Zampieri, L., Turolla, R., Zane, S., & Treves, A. 1995, *ApJ*, 439, 849
- Zane, S., Turolla, R., & Treves, A. 1998, *ApJ*, 501, 258
- Zavlin, V. E., Pavlov, G. G., & Shibunov, Yu. A. 1996, *A&A*, 315, 141
- Zdunik, J. L. 2002, *A&A*, 394, 641
- Zeldovich, Ya.B., & Novikov, I.D. 1971, *Relativistic Astrophysics* (Chicago: Univ. Chicago Press)
- Zhang, Y. 1988, *Phys. Lett. A*, 128, 309

Fig. 1.— Upper limits on the temperature of a thermal component of emission as observed at infinity for the nine models discussed in the text. The filled circles correspond to the limits summarized in column 7 of Table 1 and to an adopted maximum column density of  $N_{\text{H}} = 1.6 \times 10^{20} \text{ cm}^{-2}$  (§2); these are the temperature limits considered throughout this work. More stringent limits that correspond to the most probable column density of  $N_{\text{H}} = 1.2 \times 10^{20} \text{ cm}^{-2}$  (§2) are indicated by the cross symbol.

Fig. 2.— (a) Upper limits on the luminosity at infinity, where  $L_{\infty,\text{th}} = 4\pi R^2 \sigma T_{\text{eff}}^4 / (1+z)^2$ . The limits assume the maximum adopted column density of  $N_{\text{H}} = 1.6 \times 10^{20} \text{ cm}^{-2}$  and correspond to the 99% level of confidence. (b) Upper limits on the luminosity at the surface of the star.

Fig. 3.— A comparison of six atmospheric models for compact stars to a multiwavelength spectrum of J1118, which was published previously (MNG03). The three models with the largest peak fluxes correspond to  $\log T_{\infty} = 5.15$ , and the three less-luminous models correspond to  $\log T_{\infty} = 5.05$ . The six models cover the full range of compactnesses considered in the text and in Table 1: solid lines, Model 1 ( $\log R/R_s = 9/8$ ); dotted lines, Model 4 ( $\log R/R_s = 0.20$ ); and dashed lines, Model 9 ( $\log R/R_s = 0.45$ ). The heavy horizontal line on the right is the best-fit model X-ray spectrum, and the flanking lines define the 90% confidence error box. The UV/optical spectrum is shown on the left. Most relevant is the STIS FUV spectrum centered at  $\sim 2 \times 10^{15} \text{ Hz}$ ; these data were obtained in a 14 ks observation with STIS using the G140L grating. A firm limit on the sensitivity of this observation is indicated by the upward arrow. This limit is centered at the peak response of STIS and corresponds to the flux at  $1300\text{\AA}$  in a  $100\text{\AA}$  band; it was computed using HST’s web-based Exposure Time Calculator and assumes average background levels. HST would fail to detect a source at this limit (i.e., signal-to-noise ratio  $< 2$ ).

Fig. 4.— Eddington-scaled luminosities of BH LMXBs (filled circles) and NS LMXBs (open circles) vs. the orbital period for the energy range 0.5–10 keV. The filled square shows the upper limit on the total flux of J1118 discussed in §5.2. Only the lowest quiescent detections or *Chandra/XMM* upper limits are shown. The diagonal hatched areas delineate the regions occupied by the two classes of sources and indicate the dependence of luminosity on orbital period. Note that BH LMXBs are on average nearly three orders of magnitude fainter than NS LMXBs with similar orbital periods.

Fig. 5.— Same as Figure 3 but without the Eddington scaling. In this representation, BH LMXBs are on average a factor  $\sim 100$  fainter than NS LMXBs with similar orbital periods.

Fig. 6.— Scaled emergent flux vs. scaled frequency for various “standard” atmosphere models. Solid curves are for  $\log g = 14.1$  and (from top down) for  $\log T_{\text{eff}} = 6.0, 5.5, \text{ and } 5.0$ .

Dotted curve is the blackbody flux. Dashed curve is the approximation of equation (A17).

Fig. 7.— Temperature versus pressure for models with  $\log g = 14.654$  and  $\log T_{\text{eff}} = 6.0$ . The curves are, from bottom to top, for  $\mu_c = 0, 0.1094, 0.3522,$  and  $0.6383$ .

Fig. 8.— Solid curves are spectra for the models in Figure 8. At frequencies well below the peak, the curves are, from bottom to top, for  $\mu_c = 0, 0.1094, 0.3522,$  and  $0.6383$ . Note that the first two are barely distinguishable. Dotted curve is the blackbody flux.

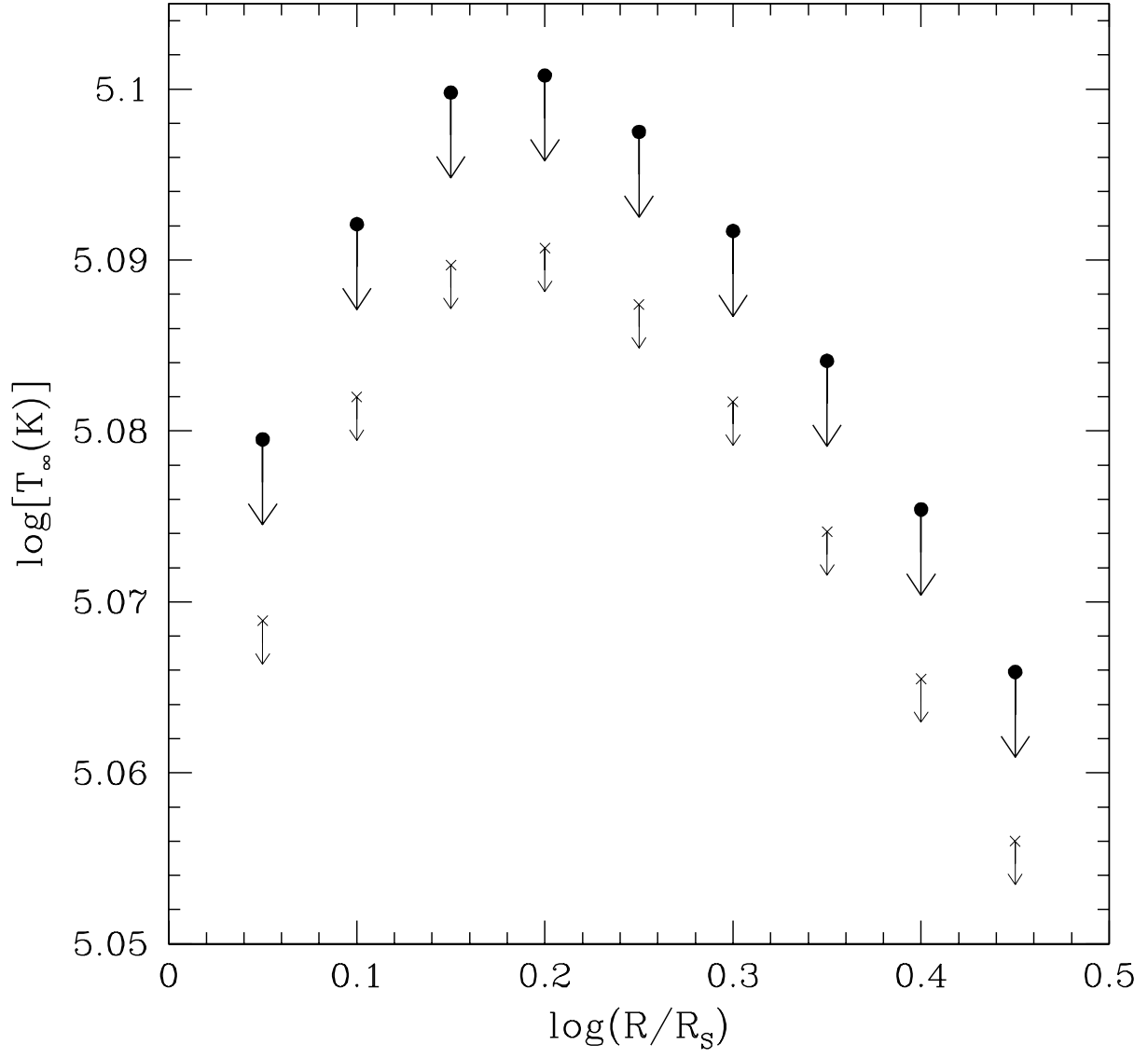


Fig. 1.—

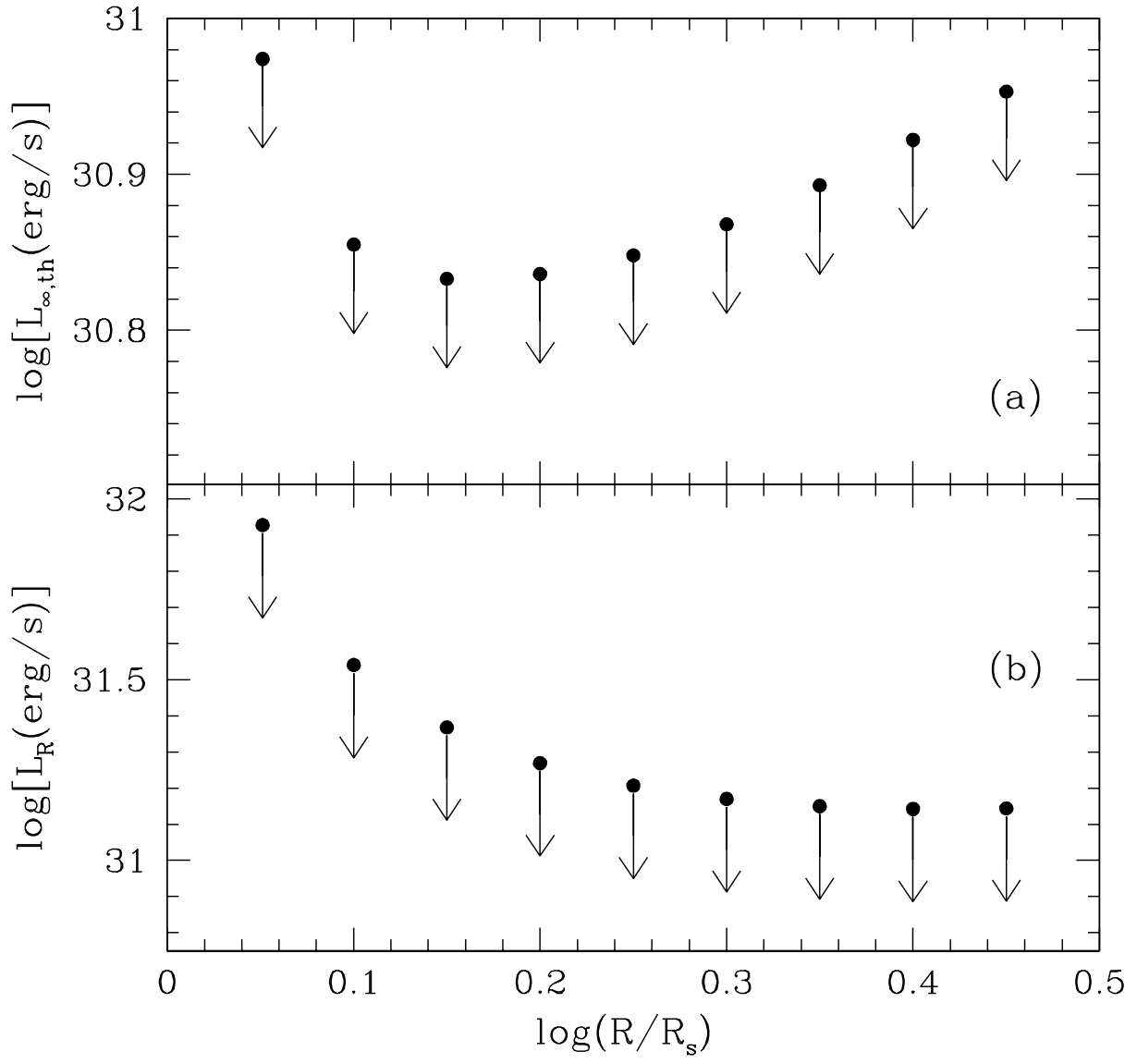


Fig. 2.—

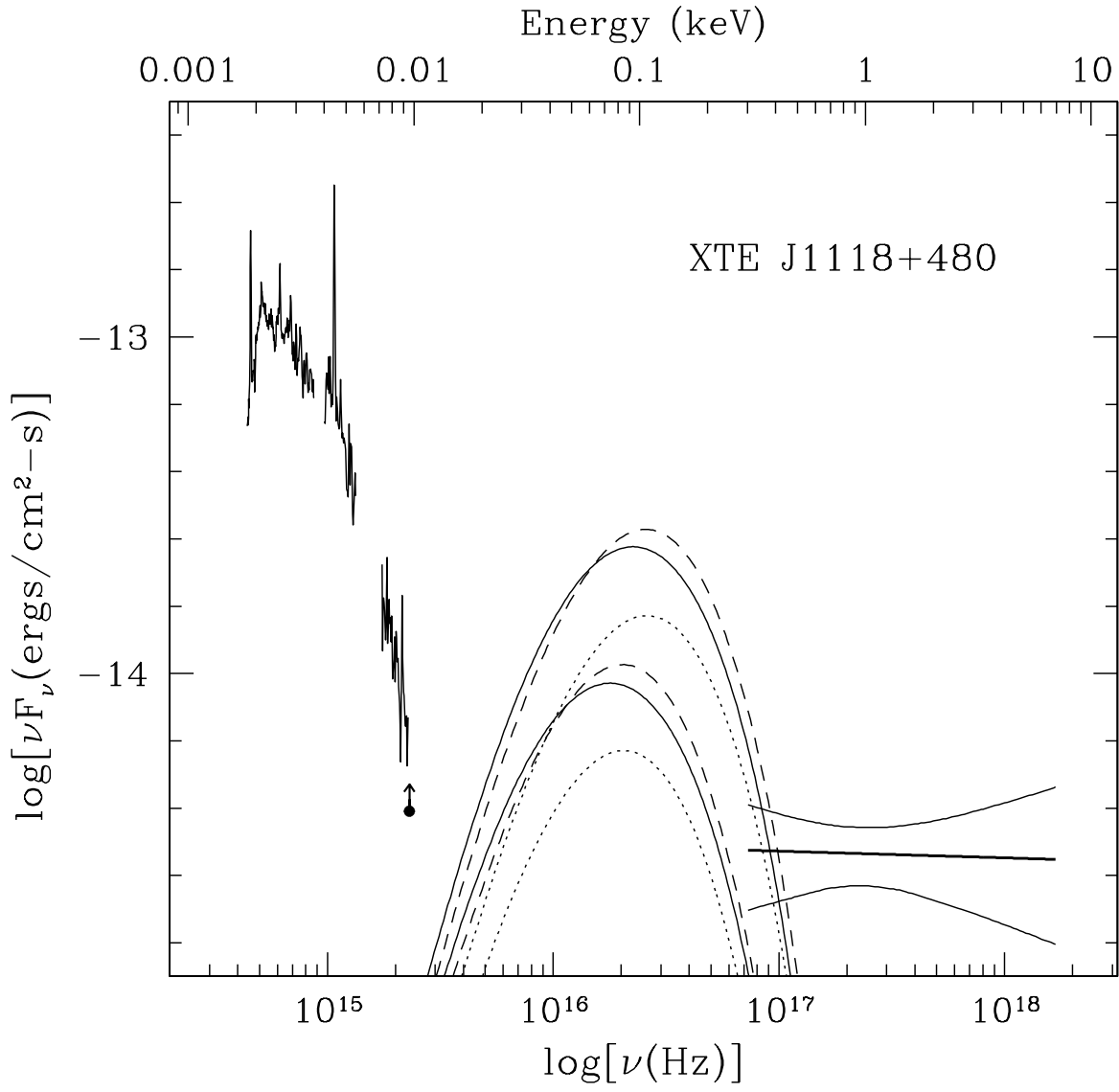


Fig. 3.—

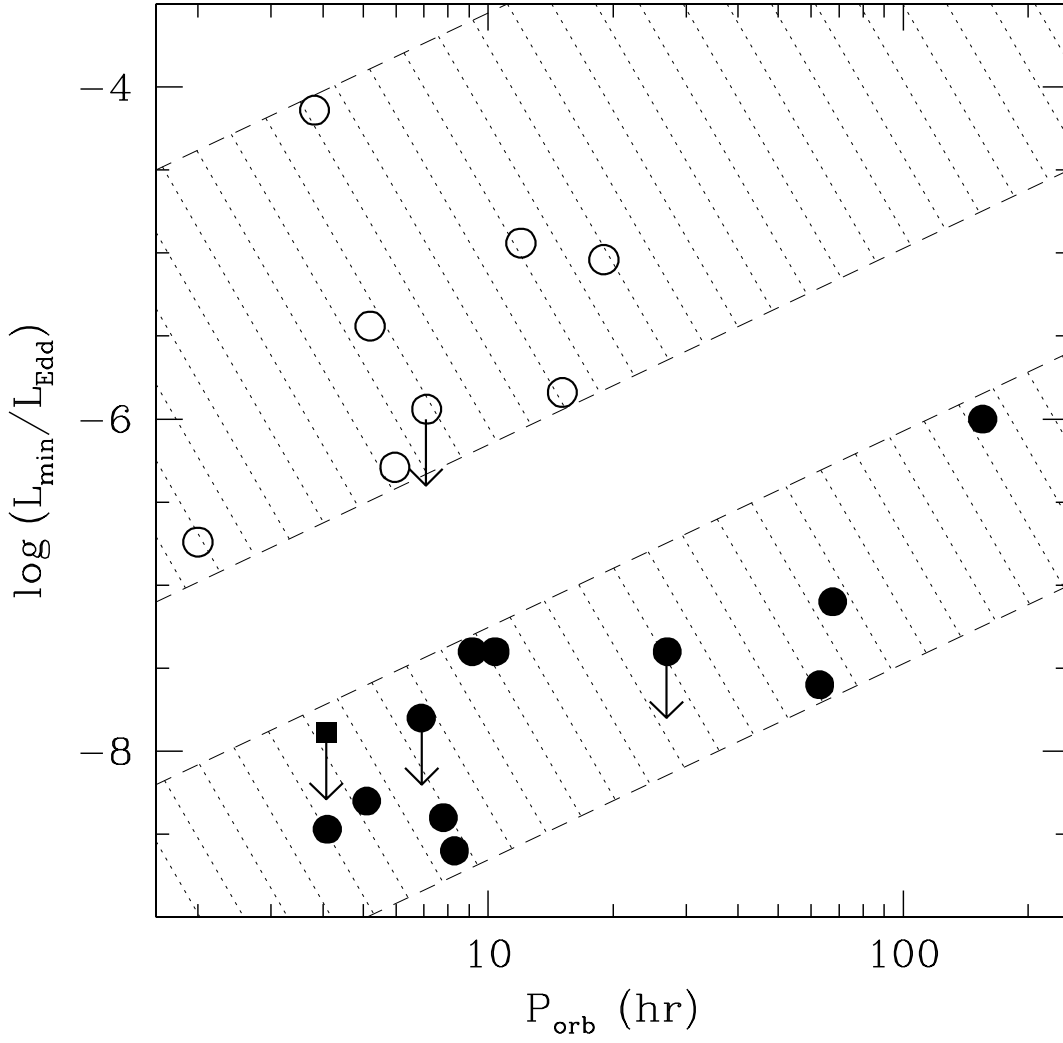


Fig. 4.—

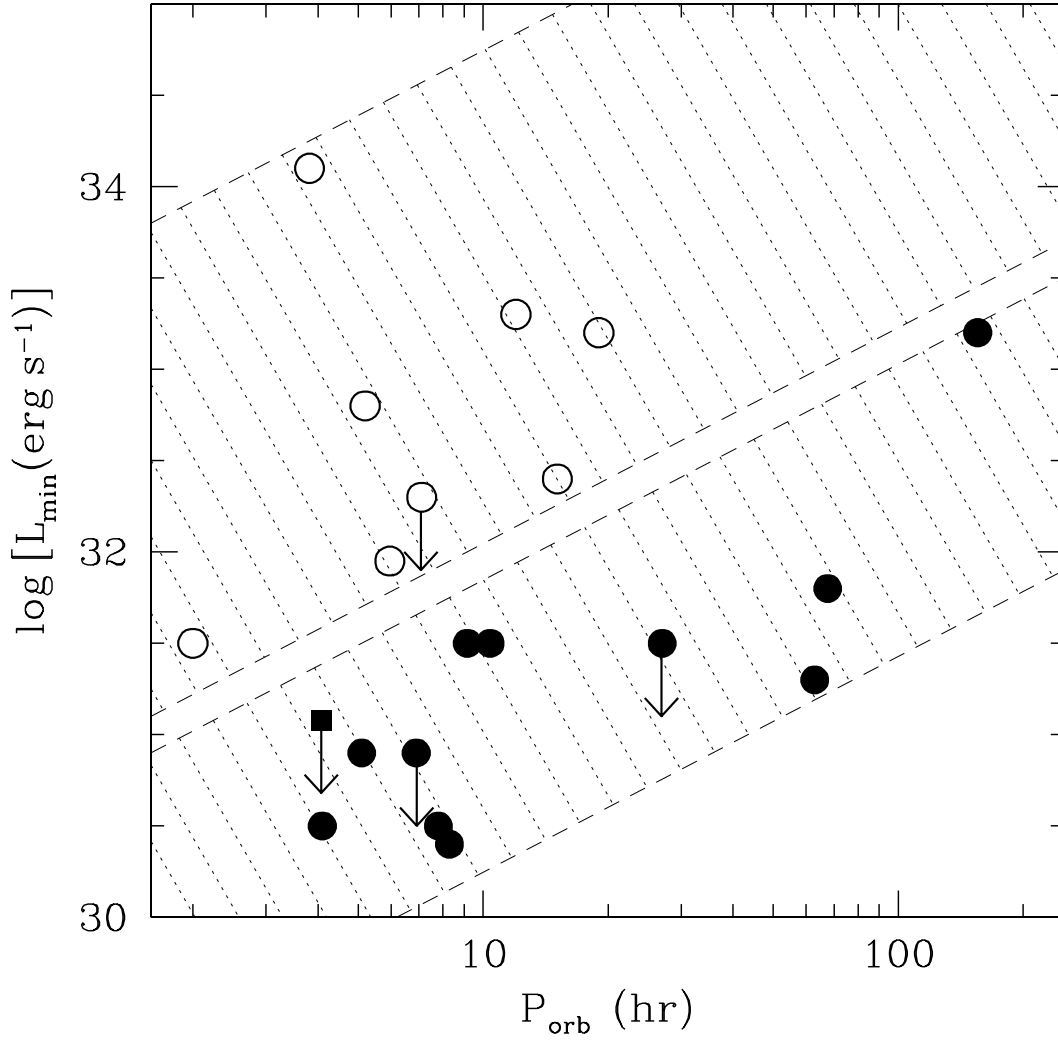


Fig. 5.—

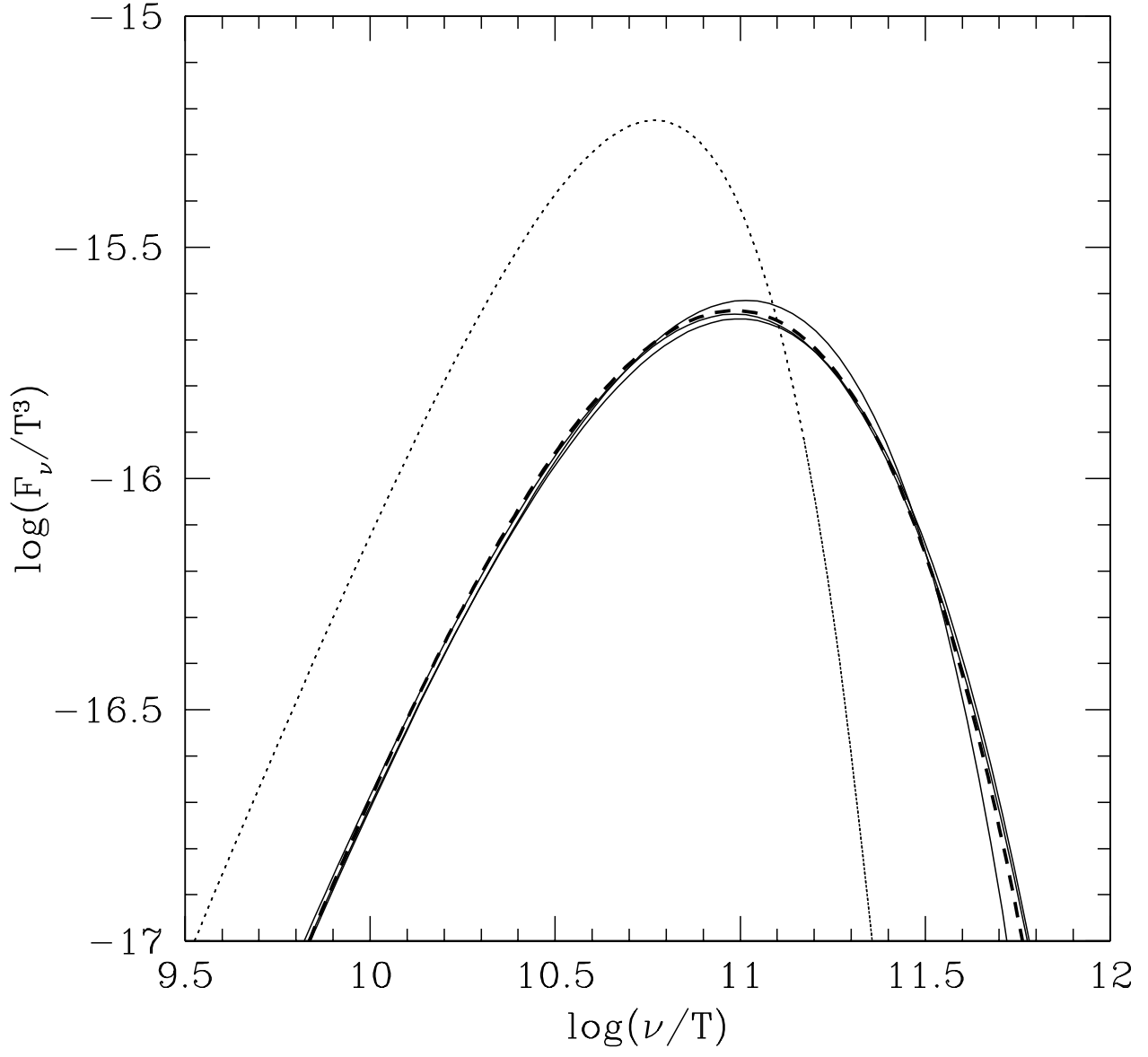


Fig. 6.—

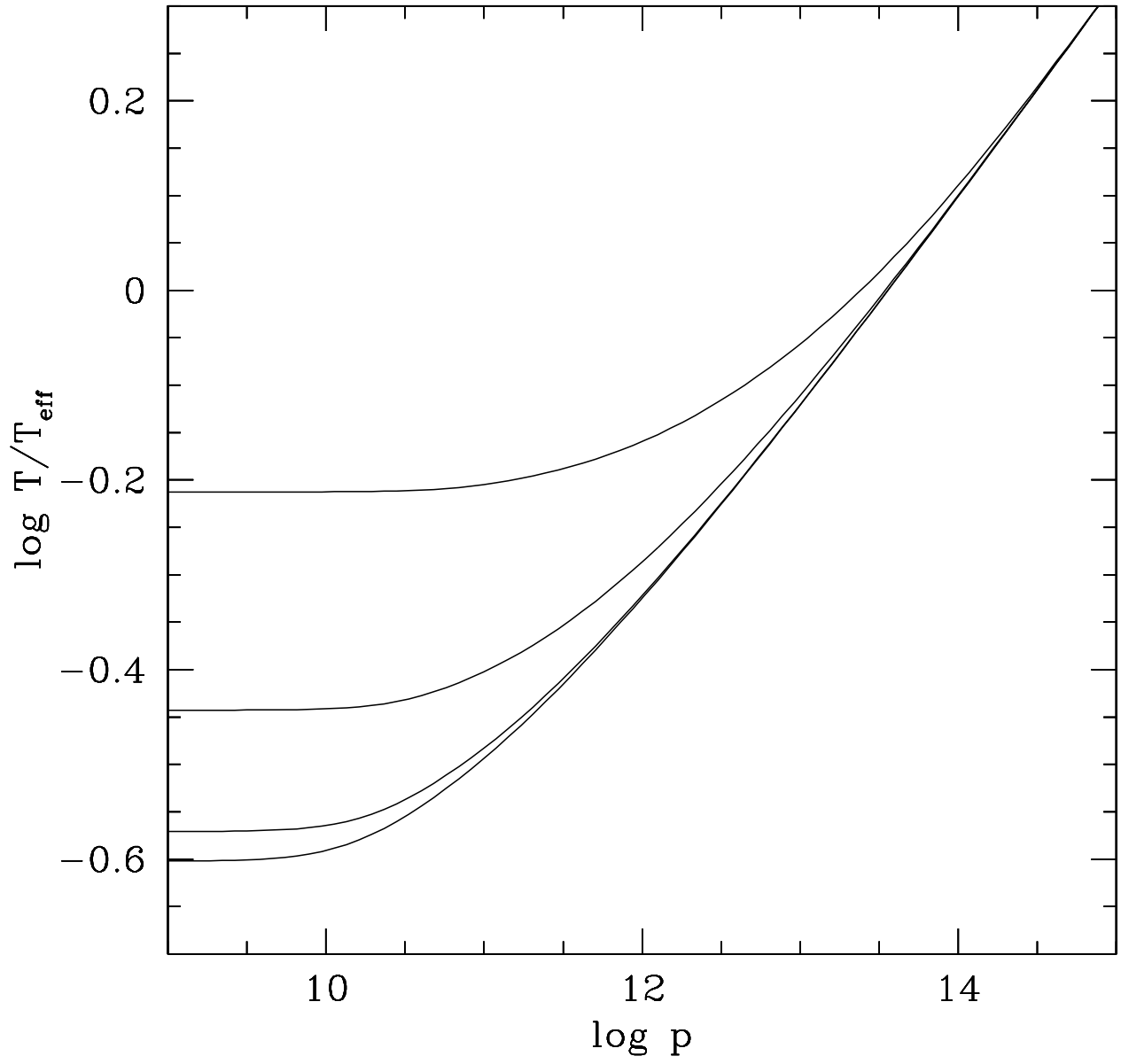


Fig. 7.—

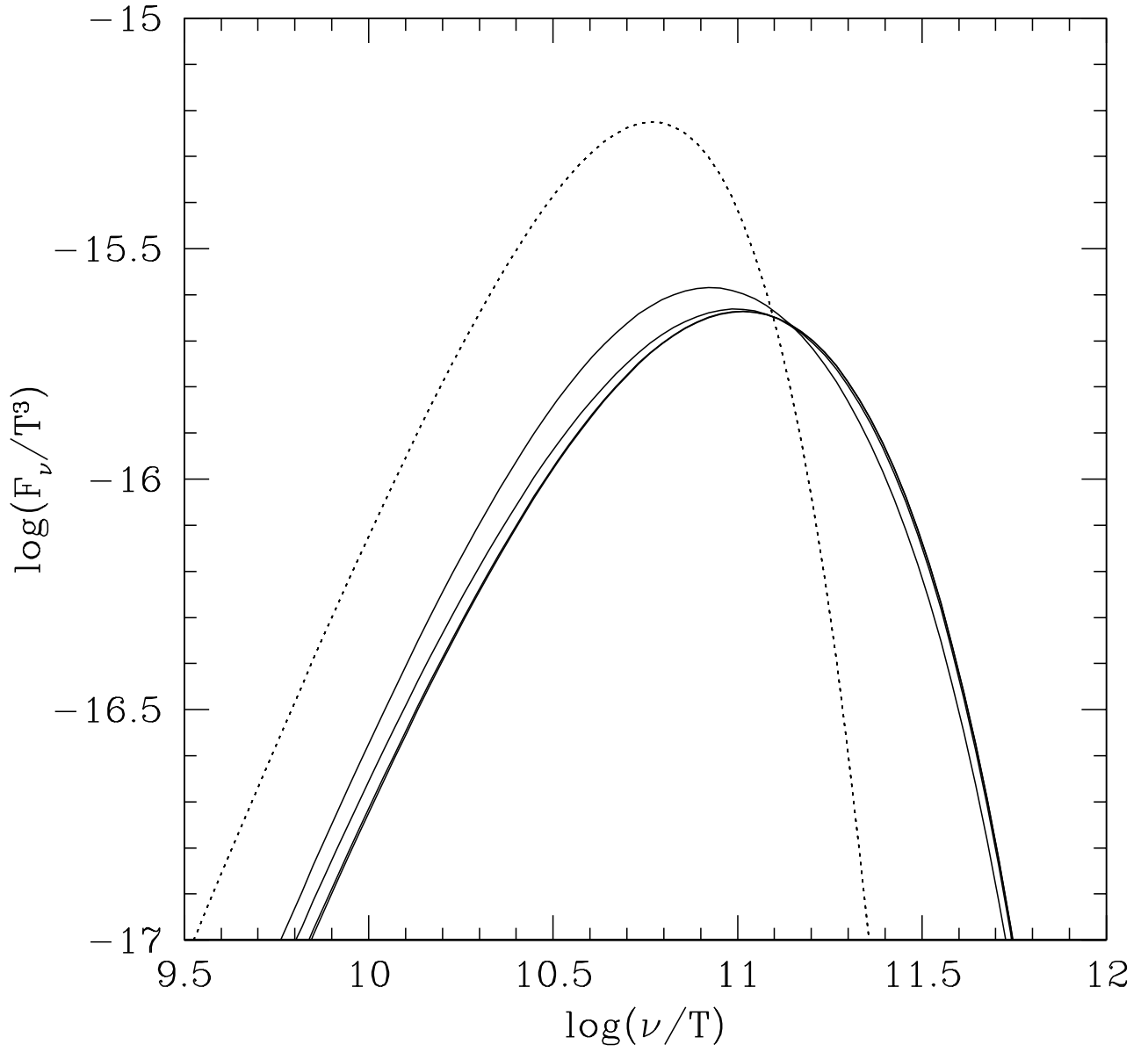


Fig. 8.—